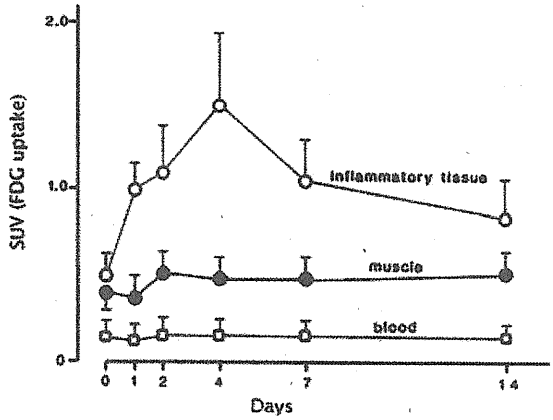

Figure 2. The time course of FDG uptake in inflammatory tissue, muscle, and blood several days after inoculation with turpentine oil. A control group without the inoculation was designated as day 0 ($n = 5$, each day after inoculation).[9]

neutrophils and macrophages, followed by that in the neutrophil layer and granulation tissue. Our results indicated that FDG PET may be useful in detecting and monitoring chronic inflammatory processes.[9]

These studies clarified the distribution of FDG both in tumors and inflamed tissues at the cellular level. Recently, the molecular processes occurring within these cells have also been clarified. Cramer *et al.* reported that the activation of hypoxia inducible factor one alpha (HIF-1α) is essential for myeloid cell infiltration and activation *in vivo*.[10] They showed that HIF-1α is essential for the regulation of the glycolytic capacity of myeloid cells; when HIF-1α is knocked out, the cellular ATP pool decreases drastically. This metabolic defect results in the profound impairment of myeloid cell aggregation, motility, invasiveness, and bacterial killing at sites of inflammation where the tissue environment is hypoxic. Thus, HIF-1α has a direct regulatory effect on both survival and function in inflammatory microenvironments. Furthermore, the rise in glycolysis in activated macrophages results in an elevation in FDG uptake. Regarding the molecular mechanisms responsible for the regulation of glycolysis, HIF-1α affects both glucose transporter and hexokinase in tumors and inflamed tissues.[11]

Rheumatoid arthritis (RA) and FDG uptake: basic research

RA is an autoimmune disorder of unknown etiology and is characterized by systematic, symmetric, and erosive synovitis.[12] RA synovitis exhibits massive leukocyte infiltration, proliferative synovial membranes, and neovascularization, giving rise to a synovial proliferative fibrovascular tissue known as a pannus. Such pannus formation is directly responsible for cartilage and bone destruction.[13,14]

The mechanism of [^{18}F]FDG accumulation has been evaluated in some inflammatory diseases, such as arteriosclerosis,[15] soft tissue abscess,[16] and pulmonary inflammation.[17] In these processes macrophages and neutrophils have been shown to be the main inflammatory cells associated with [^{18}F]FDG uptake. Lin *et al.* reported a correlation between [^{18}F]FDG uptake and the synovial tumor necrosis factor-alpha (TNF-α) concentration using a rabbit model of acute inflammatory arthritis.[18] However, the processes responsible for the accumulation of [^{18}F]FDG in the inflammatory sites involved with RA, the types of cells that play a major role in the incorporation of [^{18}F]FDG, and the mechanisms by which inflammatory reactions affect the accumulation of [^{18}F]FDG have not been intensively evaluated.

Recently, Matsui *et al.*[19] reported the mechanism of [^{18}F]FDG accumulation in RA using a murine collagen-induced arthritis (CIA) model *in vivo* as well as [^{3}H]FDG uptake by various cell types *in vitro*. They showed that [^{18}F]FDG accumulation increases with the progression of joint swelling. [^{18}F]FDG uptake begins in the area where inflammatory cell infiltration and synovial cell hyperplasia are visible, and areas of strong uptake correspond to areas where mixed cellular patterns of macrophages and fibroblasts as well as bone destruction by mature osteoclasts are often visible. These findings indicate that [^{18}F]FDG accumulation reflects the characteristic changes of pathological progression, such as pannus formation and bone destruction. Based upon *in vitro* experiments, Matsui *et al.* suggested that the cell types responsible for [^{3}H]FDG uptake are activated macrophages and proliferating fibroblasts in the presence of cytokine stimulation and hypoxic circumstances within a joint. Hypoxia is a microenvironmental feature in inflamed joints.[20] Under hypoxic conditions, macrophages begin to adopt a glycolytic metabolism[21] and release significant amounts of cytokines, such as TNF-α.[22] Neutrophils also take in [^{3}H]FDG, depending on the number of invading cells, but [^{3}H]FDG uptake in these cells is not accelerated by cytokine

stimulation or hypoxic conditions.[19] On the other hand, T cells show little [^{3}H]FDG uptake, compared with other inflammatory cells, even in the presence of cytokines.[19] B cells, which are often observed in human rheumatoid synovitis (where they form germinal centers in the region of rheumatoid synovitis and proliferate *in situ*),[23] were not observed in this CIA model. Because B cells accumulate [^{18}F]FDG under proliferative conditions,[24] the involvement of ectopic germinal centers of such proliferating B cells likely contributes to [^{18}F]FDG accumulation in rheumatoid synovitis in human RA. However, such speculations remain unconfirmed. Matsui's report indicated that [^{18}F]FDG provides information that reflects the inflammatory activity and pathological progression of RA, as further demonstrated in the clinical studies reviewed below.

FDG PET in patients with RA

Palmer *et al.* reported their pioneer work on the use of FDG PET in patients with RA for the first time in 1995.[25] They prospectively compared gadolinium-enhanced MRI and FDG PET images of wrist lesions in 12 patients receiving anti-inflammatory therapy. The patients were examined three times: before therapy and subsequently at two and 12 weeks after the start of treatment. Despite the poor anatomic resolution of FDG PET for the wrist, they performed side-by-side comparisons of the PET and MRI images and found that the region of greatest FDG uptake on the PET images corresponded to the site of an enhancing pannus on the MRI images. The volume of the enhancing pannus (VEP) was determined using fat-suppressed MRI sequences, and the total uptake value (TUV) of the wrist and the regional uptake value (RUV; approximately equivalent to the SUV_{max}) were calculated. When the data from the baseline, second, and third examinations were combined, strong linear relationships between the VEP and both the RUV and the TUV were observed. Individual evaluations at each time point and the changes between the baseline and both the second and third examinations showed similar close correlations between the VEP and both the RUV and the TUV. The VEP and FDG uptake were strongly associated with the clinical findings in the wrists, but not with the treatment outcomes. Hence, this study clarified that the major focus of inflammation in RA, which corresponded to the area of synovial hypertrophy known as a pannus, showed the highest FDG uptake in the wrist, and the FDG uptake strongly correlated with the pannus volume measured by MRI.

Beckers *et al.* reported a more extensive study that characterized FDG uptake in patients with RA. They analyzed FDG uptake in 356 joints in 21 patients with active RA including the knee, wrist, metacarpophalangeal (MCP)/proximal interphalangeal (PIP) joints, ankle, and metatarsophalangeal joints. All the clinical parameters, including the disease activity score (DAS),[28] swelling and tenderness, ultrasonography (US) findings for synovitis and synovial thickening, power Doppler studies for neovascularization, ESR, and CRP, were strongly correlated with the FDG uptake in the joints. The metabolic activity was significantly increased in the diseased joints of patients with RA. The FDG PET results were correlated with validated clinical methods for assessing disease activity. Thus, the authors concluded that PET was a suitable and quantitative method for clinically evaluating patients with RA.[26]

The authors then extended their study to include evaluations of the response to therapy. Sixteen knees in 16 patients with active RA were assessed using PET, dynamic MRI, and US at baseline and at four weeks after the initiation of anti-TNF-α treatment. The serum levels of CRP and matrix metalloproteinase-3 (MMP3) were also measured. Significant differences in the MRI and US findings were observed between the FDG PET-positive[11] and FDG PET-negative[5] patients, whereas the serum CRP and MMP-3 levels were not significantly different between these groups. Changes in the SUVs after four weeks were correlated with the changes in the MRI parameters and in the serum CRP and MMP-3 levels, but not with the changes in synovial thickness observed using US. They showed sensitive responses in FDG uptake at four weeks after anti-TNF-α therapy, suggesting that metabolic changes are likely to precede morphological changes in synovial thickness observed using US.[27]

Goerres *et al.* reported the use of whole-body FDG PET for the assessment of anti-TNF-α treatment in patients with RA. Seven patients with active RA underwent whole-body FDG PET imaging and a clinical assessment before and after undergoing anti-TNF-α therapy. The authors then evaluated FDG uptake visually using a scoring system from 0 to 4 for more than 28 joints. Among the five responders, the decrease in FDG uptake in the joints

corresponded to the decrease in inflammatory activity, as measured clinically. The two nonresponders showed a concordant increase in the disease activity visible using FDG PET and the results of the clinical evaluations in 41% of the joints. Thus, the visual assessment of FDG uptake was found to significantly correlate with clinical evaluations of disease activity in patients with RA undergoing anti-inflammatory treatment.[28]

Whole-body FDG PET/CT for patients with RA: our study

The recent development of biological agents, such as antitumor necrotic factor alpha (TNF-α) blocking agents, for the treatment of RA has revolutionized treatment strategies by aiming for complete remission. To optimize results, the timing of this expensive but powerful therapy has become important, enhancing the value of accurate evaluations of arthritic inflammatory activity.[29] Magnetic resonance imaging (MRI), especially for finger lesions, enables synovial inflammation to be delineated as contrast-enhanced lesions with excellent anatomical resolution.[30] However, arthritis in patients with RA often involves not only the fingers, but also large joints throughout the whole body. Unfortunately, the application of MRI to multiple joint lesions is not practical.

FDG uptake in patients with RA has been shown to reflect the activity of synovial inflammation.[19,25–28] Most previous studies have evaluated RA in the fingers, wrist, and knee joints, and the application of whole-body PET combined with computed tomography (CT) for the evaluation of inflammatory activity in large joints has not yet been well studied in patients with RA. We have studied FDG PET/CT to delineate large-joint lesions, including the atlanto-axial joint, in patients with RA and examined the correlation between FDG uptake and markers or symptoms of inflammation.[31]

Methods

Between May 2006 and April 2008, 18 patients (17 women, 1 man; mean age, 67 ± 11 years) with RA who met the RA criteria of the American Rheumatism Association[32] were enrolled in our study. One hour after FDG injection, PET/CT imaging from the vertex to the knee joints (with the arms in a downward position) was performed using a dedicated PET/CT scanner (Biograph 16, Siemens, Erlangen, Germany). FDG uptake in bilateral knees, hips, carpals, wrists, elbows, and shoulder joints, as well as the atlanto-axial joint (total of 13 joints) and bilateral axillary lymph nodes, was evaluated using the maximum standardized uptake value (SUV_{max}). FDG uptake was also visually evaluated using the following scoring system: 0, no uptake (same as in bone); 1, slight uptake; 2, moderate uptake (same as in liver); 3, higher than in liver; 4, highest uptake (over SUV 4). This system was modified from the scoring system reported by Goerres *et al.*[28]

Table 1. FDG uptake by painful/swollen joints and joints that are not painful/swollen[31]

	FDG uptake sore/joint	SUV_{max}/joint
Painful/swollen joints ($n = 55$)	2.96 ± 0.80	5.53 ± 3.89
Joints that are not painful/swollen ($n = 179$)	1.29 ± 0.64	2.09 ± 0.77

Mean and SD per joint.
$P < 0.001$ for each parameter in both joint groups.

Results

Regarding the RA disease status, four patients were in remission according to the criteria for RA remission,[33] and 14 patients had active arthritis (including three who were examined soon after onset). FDG uptake by the large joints, the total joints score, the total joints SUV_{max}, and the mean number of joints per patient with an FDG uptake score of 2 or more were significantly different between the patients in remission and the patients with active arthritis. The mean number of joints per patient with an FDG uptake score of 2 or more was significantly higher than the mean number of painful/swollen joints. Also, the FDG uptake score and the SUV_{max} of the painful/swollen joints were significantly higher than those of the joints that were not painful/swollen (Table 1).

Figure 3A shows a typical FDG PET/CT image of large joints with arthritis in a patient with recurrent RA. A maximum intensity projection (MIP) image showed elevated FDG uptake in multiple large joints. The wrist, elbow, and knee joints can be easily interpreted in detail using the coronal and axial

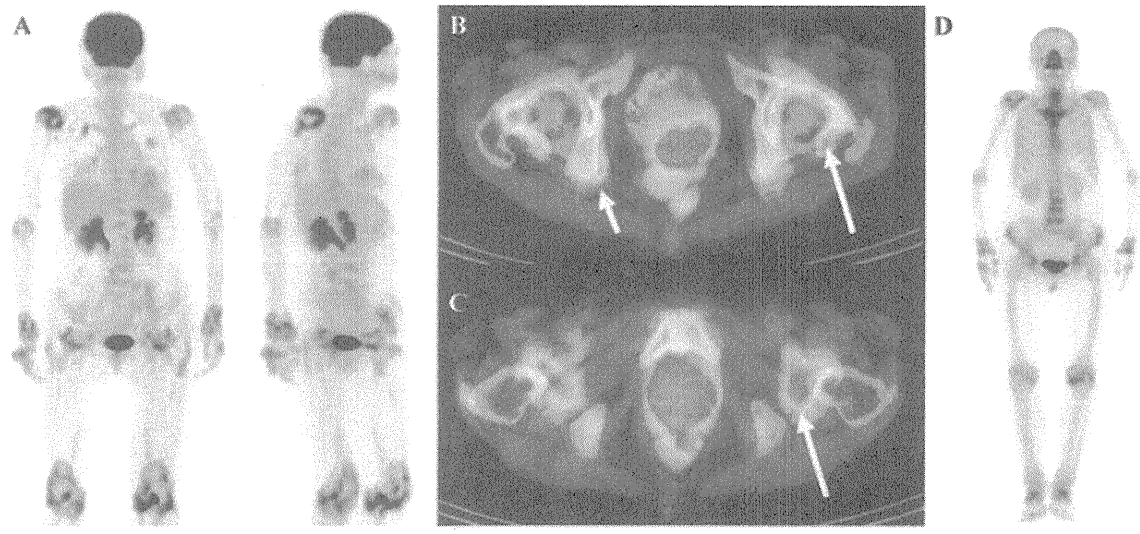

Figure 3. A 74-year-old woman with 3.5-year history of RA who experienced a recurrence and was being considered for infliximab therapy. (A) Anterior and RAO MIP image obtained using FDG-PET/CT shows typical RA lesions in the large joints. (B and C) Axial PET/CT fusion image of the hip joint in the same patient. The large arrows indicate synovitis in the acetabulum and femoral head. The small arrows indicate enthesopathies at the ischium and greater trochanter.[31] (D) Bone scan of the same patient shows mild changes in the joints.

PET views even without the CT correlation. However, the large joints, especially the hip and shoulder joints, are anatomically more complicated, and the FDG uptake by enthesopathies must be discriminated from synovitis arising from RA (Figs. 3B and C). Thus, PET images with an anatomical correlation to CT findings are essential for the accurate evaluation of synovitis arising from RA in these large joints. The bone scans of the same patients showed mild changes in the large joints, suggesting that this modality was not as sensitive as FDG PET (Fig. 3D). The CT correlation is also important for examination of the atlanto-axial joint lesion. Figure 4 shows the FDG PET/CT images obtained in another patient. Both the MIP image (Fig. 4A) and the axial images (Fig. 4B) showed typical FDG uptake in the atlanto-axial joint and axillary lymph nodes in addition to the large joint lesions. Figure 5A shows the correlation between the CRP levels and the total FDG score. The CRP level and the total FDG score exhibited a significant linear correlation (Fig. 5A, $r = 0.658$, $P = 0.003$, $n = 18$), while the CRP level and the total SUV_{max} were weakly, but not significantly, correlated ($r = 0.377$, $P = 0.123$). The WBC count was not found to correlate with the FDG uptake. A significant correlation between the total FDG uptake scores for the arm joints (summed scores of carpal, elbow, and glenohumeral joints) and the axillary lymph nodes was observed ($r = 0.731$, $P = 0.000004$, $n = 36$). FDG uptake by the axillary lymph nodes may reflect the inflammatory activity of the arm joints.[34,35] FDG uptake in the atlanto-axial joint was observed in five patients (5/18, 28%). Figure 5B shows the significant correlation between the total FDG uptake score and the FDG uptake in the atlanto-axial joint ($r = 0.669$, $P = 0.0024$, $n = 18$).

Discussion

In this study, whole-body FDG PET/CT clearly delineated RA lesions in large joints by showing the metabolic activity of inflammation overlaid on the joint anatomy revealed by CT. FDG uptake in the large joints, as evaluated using a visual scoring system, was significantly correlated with the CRP level but not with the WBC count. PET/CT also showed a higher FDG uptake in painful/swollen joints, and both of these parameters were strongly correlated with each other. These findings suggest that whole-body FDG PET/CT is sensitive in reflecting the disease activity in large joints affected by RA.

Beckers *et al.*[26,27] studied finger and knee lesions in patients with RA by measuring the SUV_{max} and found a strong correlation between

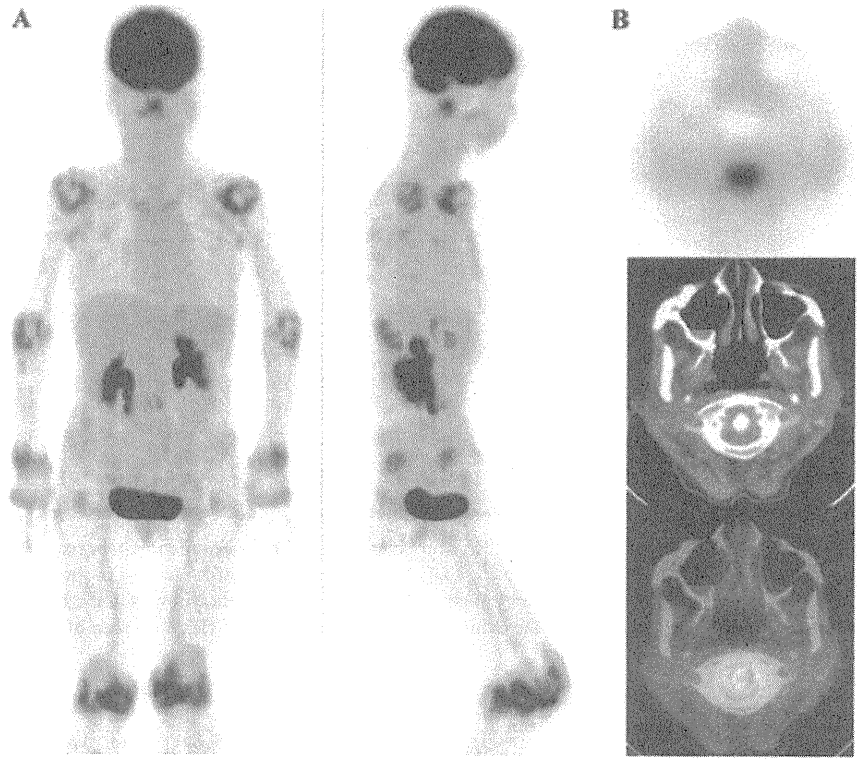

Figure 4. A 71-year-old woman with a seven-year history of RA who experienced a recurrence. (A) Anterior and right lateral views of MIP images obtained using FDG PET/CT. Strong FDG uptake was seen in the atlanto-axial joint, bilateral axillary lymph nodes, knees, hips, carpals, wrists, elbows, and shoulders joints.[31] (B) Axial images of the atlanto-axial joint (PET, CT, and fused image: top to bottom).

FDG uptake and markers of inflammation, such as the CRP level and the clinical DAS. In our study, the total FDG uptake score for large joints throughout the whole body showed similar correlations, but the total SUV_{max} was not as useful as in the previous publication.[26,27] This result might have arisen from an overlap of the background activity caused by, for example, FDG uptake in muscles adjacent to large painful joints. Visual evaluation is likely to overlook the background activity and any resulting artifacts. Goerres *et al.*[28] studied whole-body FDG PET imaging in patients with RA using a visual evaluation scoring system and concluded that FDG uptake significantly correlated with clinical evaluations of disease activity in patients with RA before and after treatment with Infliximab. While they clearly showed the utility of a visual scoring system, they neither calculated the total SUV_{max} nor used PET/CT. Further studies to clarify the differences between visually assessed scores and the total SUV_{max} in whole-body PET/CT is needed. A visual scoring system is a simple, practical, and clinically feasible evaluation method, and the method used to score FDG uptake in the present study (modified from the scoring system reported by Goerres *et al.*[28]) reflects both the inflammatory activity and the symptoms involving the large joints.

Our PET/CT study showed that the number of joints with increased FDG uptake was higher than the number of symptomatic joints. Also, we found that patients with a higher FDG uptake in their large joints throughout the whole body tended to have increased FDG uptake in their atlanto-axial joint. These results suggest that FDG PET can identify joints with active RA inflammation more sensitively than the clinical signs/symptoms of RA. Cervical involvement, especially of the atlanto-axial joint, can result in the compression of the spinal cord and brain stem, leading to serious complications. Neva *et al.*[36] reported that RA patients with cervical spine

subluxations cannot be distinguished based on their symptoms and that a high prevalence of asymptomatic cervical spine subluxation exists in patients with RA waiting for orthopedic surgery. Kaneta *et al.*[37] reported a case in which FDG PET/CT detected atlanto-axial joint involvement in a patient with RA. In our study, 28% of the patients showed a positive FDG uptake in their atlanto-axial joints, and most of these patients were asymptomatic. These observations may indicate the early stage of subclinical active synovitis that will ultimately progress to subluxation.

Linn-Rasker *et al.* examined the predictive value of the distribution of inflamed joints at the time of first presentation for the severity and disease course of RA based on a physical examination and various laboratory parameters. They concluded that the presence of arthritis in large joints, particularly arthritis in the knee joint, was predictive of a destructive disease course.[38] The evaluation of large joints with arthritis using whole-body FDG PET/CT may be helpful for identifying patients with RA who are at risk for a potentially severe disease course, including subluxation of the atlanto-axial joint, in whom a more intensive therapeutic intervention would be indicated. Also, FDG PET/CT may be useful for monitoring such therapies, especially those involving the use of biologic agents.

Bone scintigraphy has been used as a conventional imaging modality to evaluate RA. A few of our patients also underwent bone scintigraphy, but the small numbers of such patients assessed was not sufficient for a systemic comparison with the results of FDG PET/CT, and such a study remains to be performed. A direct comparison of the results of bone scans and PET has not been reported, while a study comparing MRI, bone scintigraphy, US, and radiography for RA in finger joints has shown that bone scintigraphy is sensitive, but not specific, for detecting bone erosion, and not sensitive for detecting synovitis.[39] Thus, FDG PET may be more sensitive for detecting synovitis and may reflect the disease activity better than bone scintigraphy.

RA is characterized by the early and frequent involvement of the proximal interphalangeal joint, the MCP joint, and the wrist joints. These joints have been extensively evaluated using MRI and have been shown to exhibit a strong correlation with the inflammatory activity of RA.[40] The recent development of low-field dedicated extremity MRI has especially facilitated the use of MRI with good accuracy.[40,41] The advantage of PET/CT in this study was that this modality enables the whole-body evaluation of inflammatory RA activity, possibly helping with the accurate evaluation of the extent of the disease even at subclinical levels. However, the indications for dedicated extremity MRI and PET/CT in patients with RA remain to be elucidated.

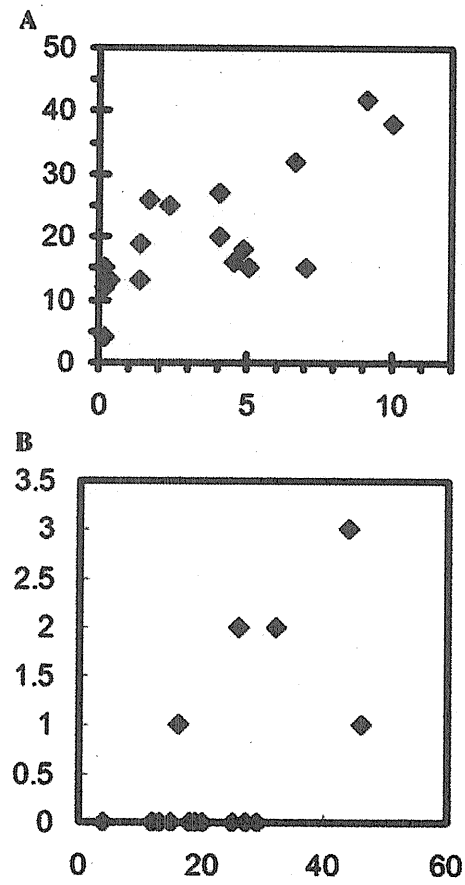

Figure 5. (A) Correlation between the CRP level (X-axis) and the total FDG uptake score in the large joints (Y-axis) ($r = 0.658$, $P < 0.01$; $n = 18$). (B) Correlation between the total FDG uptake score (X-axis) and the FDG uptake scores in the atlanto-axial joint (Y-axis) ($r = 0.669$, $P < 0.01$; $n = 18$.)[31]

Recently, a pilot study of the early evaluation with FDG PET to predict the late clinical outcome of anti-TNF-α therapy has been reported. Elzinga *et al.* performed FDG-PET studies before and two weeks after the initiation of anti-TNF-α therapy of symptomatic patients of RA. Changes in mean SUV of metacarpo-phalangeal (MP) and wrist joints at 0–2 weeks showed the best correlation with the DAS

at 14 and 22 weeks and contributed to the prediction of the clinical response. No other parameters of inflammation predicted the response.[42] They suggested the use of FDG PET for the early prediction of clinical outcome of anti-TNF-α therapy, that is, if the response is poor, noneffective expensive therapy can be stopped.

Our final goal is to demonstrate that FDG PET/CT can be useful for determining the optimal timing of anti-TNF-α therapy. To obtain compelling evidence, a multicenter prospective study involving therapeutic intervention will be necessary. We think that our study, which demonstrates the diagnostic and prognostic capabilities of whole-body PET/CT, may be one step toward achieving this goal.

Conclusion

FDG PET/CT accurately and sensitively reflects the inflammatory activity of affected joints in patients with RA and may be helpful for the early evaluation of the extent of RA throughout the whole body, including high-risk lesions such as those in the atlantoaxial joint. FDG PET/CT can also be used to evaluate the response to treatment with drugs that modify cellular activity during the fibrovascular proliferative processes leading to pannus formation. These unique capabilities of FDG PET/CT imaging may indeed be helpful in the management of patients with RA.

Acknowledgments

We would like to thank Dr. A. Nakatani of the Research Center of Nihon Medi-physics Co., Ltd., for his helpful advice. Part of this study was supported by a Grant-in-Aid for Scientific Research (C) (No. 22591362) from the Ministry of Education, Culture, Sports Science, and Technology (Japan), and by a Grant (21A126) from the National Center for Global Health and Medicine (Japan).

Conflicts of interest

The authors report no conflicts of interest.

References

1. Kubota, K. 2001. From tumor biology to clinical PET: a review of positron emission tomography (PET) in oncology. *Ann. Nucl. Med.* **15:** 471–486.
2. Fletcher, J.W., B. Djulbegovic, H.P. Soares, *et al.* 2008. Recommendations on the use of 18F-FDG PET in oncology. *J. Nucl. Med.* **49:** 480–508.
3. Boellaard, R., M.J. O'Doherty, W.A. Weber, *et al.* 2010. FDG PET and PET/CT: EANM procedure guidelines for tumour PET imaging: version 1.0. *Eur. J. Nucl. Med. Mol. Imaging* **37:** 181–200.
4. Tahara, T., Y. Ichiya, Y. Kuwabara, *et al.* 1989. High [^{18}F]fluorodeoxyglucose uptake in abdominal abscess: a PET study. *J. Comput. Assist. Tomogra.* **13:** 829–831.
5. Sasaki, M., Y. Ichiya, Y. Kuwabara, *et al.* 1990. Ring-like uptake of [18F]FDG in brain abscess: a PET study. *J. Comput. Assist. Tomogra.* **14:** 486–487.
6. Kubota, K., T. Matsuzawa, T. Fujiwara, *et al.* 1990. Differential diagnosis of lung tumor with positron emission tomography: a prospective study. *J. Nucl. Med.* **31:** 1927–1933.
7. Kubota, R., S. Yamada, K. Kubota, *et al.* 1992. Intratumoral distribution of fluorine-18-fluorodeosxyglucose *in vivo*: high accumulation in macrophages and granulation tissues studied by microautoradiography. *J. Nucl. Med.* **33:** 1972–1980.
8. Kubota, K., R. Kubota & S. Yamada. 1993. FDG accumulation in tumor tissue. *J. Nucl. Med.* **34:** 75–82.
9. Yamada, S., K. Kubota, R. Kubota, *et al.* 1995. High accumulation of fluorine-18-fluorodeoxyglucose in turpentine-induced inflammatory tissue. *J. Nucl. Med.* **36:** 1301–1306.
10. Cramer, T., Y. Yamanishi, B.E. Clausen, *et al.* 2003. HIF-1 is essential for myeloid cell-mediated inflammation. *Cell* **112:** 645–657.
11. Denko, N.C. 2008. Hypoxia, HIF1 and glucose metabolism in the solid tumour. *Nat. Rev. Cancer* **8:** 705–713.
12. Harris, E.D. Jr. 1990. Rheumatoid arthritis: pathophysiology and implications for therapy. *N. Engl. J. Med.* **322:** 1277–1289.
13. Lee, D.M. & M.E. Weinblatt. 2001. Rheumatoid arthritis. *Lancet* **358:** 903–911.
14. Scutellari, P.N. & C. Orzincolo. 1998. Rheumatoid arthritis: sequences. *Eur. J. Radiol.* **27**(suppl. 1): S31–S38.
15. Ogawa, M., S. Ishino, T. Mukai, *et al.* 2004. (18)F-FDG accumulation in atherosclerotic plaques: immunohistochemical and PET imaging study. *J. Nucl. Med.* **45:** 1245–1250.
16. Kaim, A.H., B. Weber, M.O. Kurrer, *et al.* 2002. Autoradiographic quantification of 18F-FDG uptake in experimental soft-tissue abscesses in rats. *Radiology* **223:** 446–451.
17. Hazel, A.J., B.S. John, K. Thomas, *et al.* 1998. Pulmonary fibrosis correlates with duration of tissue neutrophil activation. *Am. J. Respir. Crit. Care Med.* **158:** 620–628.
18. Lin, P.W., R.S. Liu, T.H. Liou, *et al.* 2007. Correlation between joint [F-18] FDG PET uptake and synovial TNF-alpha concentration: a study with two rabbit models of acute inflammatory arthritis. *Appl. Radiat. Isot.* **65:** 1221–1226.
19. Matsui, T., N. Nakata, S. Nagai, *et al.* 2009. Inflammatory cytokines and hypoxia contribute to 18F-FDG uptake by cells involved in pannus formation in rheumatoid arthritis. *J. Nucl. Med.* **50:** 920–926.
20. Roiniotis, J., H. Dinh, P. Masendycz, *et al.* 2009. Hypoxia prolongs monocyte/macrophage survival and enhanced glycolysis is associated with their maturation under aerobic conditions. *J. Immunol.* **182:** 7974–7981.
21. Ng, C.T., M. Biniecka, A. Kennedy, *et al.* 2010. Synovial tissue hypoxia and inflammation *in vivo*. *Ann. Rheum. Dis.* **69:** 1389–1395.

22. Scannell, G. 1996. Leukocyte responses to hypoxic/ischemic conditions. *New Horiz.* **4:** 179–183.
23. Malone, D.G., S.M. Wahl & M. Tsokos. 1984. Immune function in severe, active rheumatoid arthritis: a relationship between peripheral blood mononuclear cell proliferation to soluble antigens and synovial tissue immunohistologic characteristics. *J. Clin. Invest.* **74:** 1173–1185.
24. Shozushima, M., R. Tsutsumi, K. Terasaki, *et al.* 2003. Augmentation effects of lymphocyte activation by antigen-presenting macrophages on FDG uptake. *Ann. Nucl. Med.* **17:** 555–560.
25. Palmer, W.E., D.J. Rosenthal, O.I. Schoenberg, *et al.* 1995. Quantification of inflammation in the wrist with gadolinium-enhanced MR imaging and PET with 2-[F-18]-fluoro-2-deoxy-D-glucose. *Radiology* **196:** 647–655.
26. Beckers, C., C. Ribbens, B. André, *et al.* 2004. Assessment of disease activity in rheumatoid arthritis with 18F-FDG PET. *J. Nucl. Med.* **45:** 956–964.
27. Beckers, C., X. Jeukens, C. Ribbens, *et al.* 2006. ^{18}F-FDG PET imaging of rheumatoid knee synovitis correlates with dynamic magnetic resonance and sonographic assessments as well as with the serum level of metalloproteinase-3. *Eur. J. Nucl. Med. Mol. Imaging* **33:** 275–280.
28. Goerres, G.W., A. Forster, D. Uebelhart, *et al.* 2006. F-18 FDG whole-body PET for the assessment of disease activity in patients with rheumatoid arthritis. *Clin. Nucl. Med.* **31:** 386–390.
29. Majithia, V. & S.A. Geraci. 2007. Rheumatoid arthritis: diagnosis and management. *Am. J. Med.* **120:** 936–939.
30. Boutry, N., M. More, R.M. Flipo, *et al.* 2007. Early rheumatoid arthritis: a review of MRI and sonographic findings. *Am. J. Roentgenol.* **189:** 1502–1509.
31. Kubota, K., K. Ito, M. Morooka, *et al.* 2009. Whole-body FDG-PET/CT on rheumatoid arthritis of large joints. *Ann. Nucl. Med.* **23:** 783–791.
32. Arnett, F.C., S.M. Edworthy, D.A. Block, *et al.* 1988. The American Rheumatism Association 1987 revised criteria for the classification of rheumatoid arthritis. *Arthritis Rheum.* **31:** 315–324.
33. 1996. [No authors listed] Guidelines for the management of rheumatoid arthritis. American College of Rheumatology Ad Hoc Committee on clinical guidelines. *Arthritis Rheum.* **39:** 713–722.
34. Seldin, D.W., I. Habib & G. Soudry. 2007. Axillary lymph node visualization of F-18 FDG PET body scan in patients with rheumatoid arthritis. *Clin. Nucl. Med.* **32:** 524–526.
35. Calgüneri, M., M.A. Oztürk, Z. Ozbalkan, *et al.* 2003. Frequency of lymphadenopathy in rheumatoid arthritis and systemic lupus erythematosus. *J. Int. Med. Res.* **31:** 345–349.
36. Neva, M.H., A. Häkkinen, H. Mäkinen, *et al.* 2006. High prevalence of asymptomatic cervical spine subluxation in patients with rheumatoid arthritis waiting for orthopaedic surgery. *Ann. Rheum. Dis.* **65:** 884–888.
37. Kaneta, T., T. Hakamatsuka, T. Yamada, *et al.* 2006. Atlantoaxial osteoarthritis in rheumatoid arthritis: FDG PET/CT findings. *Clin. Nucl. Med.* **31:** 209.
38. Linn-Rasker, S.P., A.H. van der Helm-van Mil, F.C. Breedveld & T.W.J. Huizinga. 2007. Arthritis of the large joints—in particular, the knee—at first presentation is predictive for a high level of radiological destruction of the small joints in rheumatoid arthritis. *Ann. Rheum. Dis.* **66:** 646–650.
39. Backhaus, M., T. Kamradt, D. Sandrok, *et al.* 1999. Arthritis of the finger joints: a comprehensive approach comparing conventional radiograph, scintigraphy, ultrasound, and contrast-enhanced magnetic resonance imaging. *Arthritis Rheum.* **42:** 1232–1245.
40. Hodgson, R.J., P.O. Connor & R. Moots. 2008. MRI of rheumatoid arthritis-image quantification for the assessment of disease activity, progression and response to therapy. *Rheumatology* **47:** 13–21.
41. Taouli, B., S. Zaim, C.G. Peterfy, *et al.* 2004. Rheumatoid arthritis of the hand and wrist: comparison of three imaging techniques. *Am. J. Roentgenol.* **182:** 937–943.
42. Elzinga, E.H., C.J. van der Laken, E.F.I. Comans, *et al.* 2011. 18F-FDG PET as a tool to predict the clinical outcome of infliximab treatment of rheumatoid arthritis: an explorative study. *J. Nucl. Med.* **52:** 77–80.

arthritis research&therapy

RESEARCH ARTICLE Open Access

A 4-trifluoromethyl analogue of celecoxib inhibits arthritis by suppressing innate immune cell activation

Asako Chiba[1], Miho Mizuno[1], Chiharu Tomi[1], Ryohsuke Tajima[1], Iraide Alloza[2], Alessandra di Penta[2], Takashi Yamamura[1], Koen Vandenbroeck[2,3] and Sachiko Miyake[1*]

Abstract

Introduction: Celecoxib, a highly specific cyclooxygenase-2 (COX-2) inhibitor has been reported to have COX-2-independent immunomodulatory effects. However, celecoxib itself has only mild suppressive effects on arthritis. Recently, we reported that a 4-trifluoromethyl analogue of celecoxib (TFM-C) with 205-fold lower COX-2-inhibitory activity inhibits secretion of IL-12 family cytokines through a COX-2-independent mechanism that involves Ca^{2+}-mediated intracellular retention of the IL-12 polypeptide chains. In this study, we explored the capacity of TFM-C as a new therapeutic agent for arthritis.

Methods: To induce collagen-induced arthritis (CIA), DBA1/J mice were immunized with bovine type II collagen (CII) in Freund's adjuvant. Collagen antibody-induced arthritis (CAIA) was induced in C57BL/6 mice by injecting anti-CII antibodies. Mice received 10 μg/g of TFM-C or celecoxib every other day. The effects of TFM-C on clinical and histopathological severities were assessed. The serum levels of CII-specific antibodies were measured by ELISA. The effects of TFM-C on mast cell activation, cytokine producing capacity by macophages, and neutrophil recruitment were also evaluated.

Results: TFM-C inhibited the severity of CIA and CAIA more strongly than celecoxib. TFM-C treatments had little effect on CII-specific antibody levels in serum. TFM-C suppressed the activation of mast cells in arthritic joints. TFM-C also suppressed the production of inflammatory cytokines by macrophages and leukocyte influx in thioglycollate-induced peritonitis.

Conclusion: These results indicate that TFM-C may serve as an effective new disease-modifying drug for treatment of arthritis, such as rheumatoid arthritis.

Introduction

In the past decade, a series of potent new biologic therapeutics have demonstrated remarkable clinical efficacy in several autoimmune diseases, including rheumatoid arthritis (RA). In the case of RA, a chronic progressive autoimmune disease that targets joints and occurs in approximately 0.5 to 1% of adults, biologic agents, such as TNF inhibitors, have proven effective in patients not responding to disease-modifying anti-rheumatic drugs, such as methotrexate. However, about 30% of patients treated with a TNF inhibitor are primary non-responders. Moreover, a substantial proportion of patients experience a loss of efficacy after a primary response to a TNF inhibitor (secondary non-responders) [1-3]. More recently, as new therapies have become available, including biological agents targeting IL-6, B cells and T cells, it has become clear that a notable proportion of patients respond to these new biological agents even among primary and secondary non-responders to TNF inhibitors [3-10]. These individual differences in response to each agent highlight the difficulty and limit of treating multifactorial disease by targeting single cytokine or single cell type. Patient-tailored therapy might be able to

* Correspondence: miyake@ncnp.go.jp
[1]Department of Immunology, National Institute of Neuroscience, National Center of Neurology and Psychiatry, 4-1-1 Ogawahigashi, Kodaira, Tokyo 187-8502, Japan
Full list of author information is available at the end of the article

overcome this issue, but good biomarkers to predict treatment responses have not yet been elucidated.

Therefore, as described above, biological drugs have limited values. In addition, such drugs may be accompanied by serious side effects [11,12]. Furthermore, the high cost of these biological drugs may make access to these reagents prohibitive for the general public. Alternative therapeutic options, such as small molecule-based drugs, continue to be an important challenge.

The involvement of prostaglandin pathways in the pathogenesis of arthritis has been shown in animal models by using mice lacking genes, such as cycolooxygenase-2 (COX-2), prostaglandin E synthase, or prostacyclin receptor [13-15]. As COX-2 knockout mice normally develop autoreactive T cells in collagen-induced arthritis (CIA) [13], prostaglandin pathways appear to be involved mainly in the effector phase of arthritis. However, treatment with celecoxib, a prototype drug belonging to a new generation of highly specific COX-2 inhibitors has been reported to have only mild suppressive effects on animal models of arthritis, and strong inhibition of arthritis was achieved only when mice were treated in the combination of celecoxib with leukotriene inhibitors [16-19]. In humans, although celecoxib is widely used as an analgesic agent in patients with RA or osteoarthritis, there is no evidence that celecoxib therapy modulates the clinical course of RA. In addition, recently it has been shown that celecoxib enhances TNFα production by RA synovial membrane cultures and human monocytes [20].

Celecoxib has been reported to exhibit COX-2-independent effects, such as tumor growth inhibition and immunomodulation [21,22]. Previously, we demonstrated that celecoxib treatment suppressed experimental autoimmune encephalomyelitis (EAE) in a COX-2 independent manner [22]. We recently developed a trifluoromethyl analogue of celecoxib (TFM-C; full name: 4-[5-(4-trifluoromethylphenyl)-3-(trifluoromet-hyl)-1*H*-pyrazol-1-yl]benzenesulfonamide), with 205-fold lower COX-2-inhibitory activity. In studies using recombinant cell lines, TFM-C inhibited secretion of the IL-12 family cytokines, IL-12, p80 and IL-23, through a COX-2-independent, Ca^{2+}-dependent mechanism involving chaperone-mediated cytokine retention in the endoplasmic reticulum coupled to degradation via the ER stress protein HERP [23,24]. In the present study, we demonstrate that TFM-C inhibits innate immune cells and animal models of arthritis, including CIA and type II collagen antibody-induced arthritis (CAIA), in contrast to the limited inhibitory effect of celecoxib. TFM-C suppresses the activation of mast cells in arthritic joints. Moreover, TFM-C treatment suppresses the production of inflammatory cytokines by macrophages and leukocyte recruitment. These findings indicate that TFM-C may serve as an effective new drug for the treatment of arthritis, including RA.

Materials and methods

Differentiation and stimulation of U937 cells

Human U937 cells were obtained from the American Type Culture Collection (Rockville, MD, USA) and cultured in RPMI 1640 supplemented with 10% FCS. To differentiate U937 cells, 5×10^5 cells were treated with PMA (25 ng/ml) for 24 hours. At 22 hours of PMA treatment, 50 μM of TFM-C was added for 2 hours. Subsequently, cells were stimulated with 5 μg/ml of LPS and PMA (25 ng/ml) for 0, 3, 6, 12 and 24 hours in the presence or absence of TFM-C. Supernatants were harvested and assayed for cytokine production by means of Quansys Q-Plex™ Array (Quansys Bioscience, Logan, Utah, USA). RNA isolation was performed following the manufacturer's instructions (Macherey-Nagel, Düren, Germany).

Quantitative RT-PCR (qPCR)

A total of 200 ng of RNA extracted from U937 cells was retrotranscribed to cDNA using random primers according to the manufacturer's protocol (Applied Biosystems, Carlsbad, California, USA). qPCR was performed with the Supermix for SsoFast EvaGreen (Biorad, Hercules, California, USA) on a 7500 Fast Real-Time PCR System (Applied Biosystems). For each target gene, qPCR QuantiTect Primer Assays were used (Qiagen Hilden, Germany). For each sample, expression levels of the transcripts of interest were compared to that of endogenous GAPDH. The levels of mRNA are calculated as 2^{-Ct}.

Quansys Q-Plex™ Array chemiluminescent

A total of 30 μl of medium from differentiated U937 cells treated with PMA/LPS/TFM-C or LPS/PMA were analyzed. Human Cytokine Stripwells (16-plex) were used following the manufacturer's instructions. The image was acquired using Bio-Rad Chemidoc camera and analyzed with Q-View Software (Quansys Bioscience, Logan, Utah, USA)

DAPI staining

Differentiated U937s were treated with LPS/PMA/TFM-C for 6, 12 and 24 hours and then fixed with 2% PFA. The cells were washed three times with PBS and then incubated with DAPI (1:50000; Molecular Probes, Carlsbad, California, USA) in PBS. Coverslips were embedded in Fluoro-Gel (Electron Microscopy Science, Hatfield, Pennsylvania, USA). Images were recorded using the ApoTome system (AxioVision, Carl Zeiss, Inc., Oberkochen, Germany) and analyzed using the ImageJ program (version 1.40, Bethesda, Maryland, USA).

AlarmBlue staining of U937 cells

The number of viable cells was tested at 6, 12, and 24 hours after TFM-C exposure by adding the AlamarBlue reagent (AbD Serotec, Cambridge, UK). Absorbance was measured at wavelengths of 570 nm and 600 nm after required incubation, using a Varioskan Flash (Thermo Fisher Scientific, Fremont, CA, USA). Absorbance values of samples were normalized with values of the cell culture media without cells. The results are presented as the proportion of viable cells, calculated by dividing the absorbance values of drug-treated samples by the absorbance values of untreated control samples.

Mice

DBA1/J mice were purchased from Oriental Yeast Co., Ltd. (Tokyo, Japan). C57BL/6J (B6) mice were purchased from CLEA Laboratory Animal Corp. (Tokyo, Japan). Animal care and use were in accordance with institutional guidelines and all animal experiments were approved by the Institutional Animal Care and Use Committee of the National Institute of Neuroscience.

Induction of CIA

DBA1/J male mice (n = 5 to 6 per group, 7 to 8 weeks old) were immunized intradermally at the base of the tail with 150 μg of bovine type II collagen (CII) (Collagen Research Center, Tokyo, Japan) emulsified with an equal volume of complete Freund's adjuvant (CFA), containing 250 μg of H37Ra *Mycobacterium tuberculosis (Mtb)* (Difco, Detroit, MI, USA). DBA1/J mice were boosted 21 days after immunization by intradermal injection with 150 μg of CII emulsified with incomplete Freund's adjuvant (IFA).

Induction of CAIA

B6 female mice (n = 5 to 6 per group, 7 to 8 weeks old) were injected intravenously with 2 mg of a mixture of anti-CII monoclonal antibodies (mAbs) (Arthrogen-CIA mAb (Chondrex. LLC. Seattle, WA, USA)), and two days later with 50 μg of lipopolysaccharide (LPS) was injected intraperitoneally.

Clinical assessment of arthritis

Mice were examined for signs of joint inflammation and scored as follows: 0: no change, 1: significant swelling and redness of one digit, 2: mild swelling and erythema of the limb or swelling of more than two digits, 3: marked swelling and erythema of the limb, 4: maximal swelling and redness of the limb and later, ankylosis. The average macroscopic score was expressed as a cumulative value for all paws, with a maximum possible score of 16.

Thioglycollate-induced peritonitis

Mice were injected with 1 ml of 4% sterile thioglycollate intraperitoneally. Four hours later, mice were killed and peritoneal lavage fluid was collected by washing the peritoneal cavity with cold PBS containing 5 mM EDTA and 10 U/ml heparin.

Administration of TFM-C or celecoxib

TFM-C and celecoxib were synthesized as previously described [23]. We injected TFM-C or celecoxib intraperitonealy (i.p.) in 0.5% Tween/5% DMSO/PBS. In CIA experiments, mice received 10 μg/g TFM-C or celecoxib every other day from 21 days after immunuization. In CAIA, we injected the mice with 10 μg/g of TFM-C or celecoxib every other day starting at two days before disease induction. In thioglycollate-induced peritonitis experiments, mice received 10 μg/g of TFM-C or celecoxib two days and one hour before thioglycollate injection. The control animals were injected with vehicle alone.

Histopathology

Arthritic mice were sacrificed and all four paws were fixed in buffered formalin, decalcified, embedded in paraffin, sectioned, and then stained with H&E. Histological assessment of joint inflammation was scored as follows: 0: normal joint, 1: mild arthritis: minimal synovitis without cartilage/bone erosions, 2: moderate arthritis: synovitis and erosions but joint architecture maintained, 3: severe arthritis; synovitis, erosions, and loss of joint integrity. The average of the macroscopic score was expressed as a cumulative value of all paws, with a maximum possible score of 12.

Mast cells in synovium were visually assessed for intact versus degranulating mast cells using morphologic criteria. Mast cells were identified as those cells that contained toluidine blue-positive granules. Only cells in which a nucleus was present were counted. Degranulating cells were defined by the presence of granules outside the cell border with coincident vacant granule space within the cell border as described previously [25].

Measurement of CII specific IgG1 and IgG2a

Bovine CII (1 mg/ml) was coated onto ELISA plates (Sumitomo Bakelite, Co., Ltd, Tokyo, Japan) at 4°C overnight. After blocking with 1% bovine serum albumin in PBS, serially diluted serum samples were added onto CII-coated wells. For detection of anti-CII Abs, the plates were incubated with biotin-labeled anti-IgG1 and anti-IgG2a (Southern Biotechnology Associates, Inc., Brimingham, AL, USA) or anti-IgG Ab (CN/Cappel, Aurora, OH, USA) for one hour and then incubated with streptavidin-peroxidase. After adding a substrate, the reaction was evaluated as OD_{450} values.

Stimulation of or macrophages

B6 mice received 10 μg/g of TFM-C or control vehicle on Day 0 and Day 2, and on Day 3, splenic macrophages were collected and were stimulated by LPS *in vitro* in the presence of TFM-C or vehicle.

Detection of cytokines

Cytokine levels in the culture supernatant were determined by using a sandwich ELISA. The Abs for IL-1β ELISA were purchased from BD Biosciences (San Jose, CA, USA) and the ELISA Abs for IL-6 and TNFα were purchased from eBioscience (San Diego, CA, USA).

Statistical analysis

CIA and CAIA clinical or pathological scores for groups of mice are presented as the mean group clinical score + SEM, and statistical differences were analyzed with a non-parametric Mann-Whitney *U*-test. Data for cytokines were analyzed by an unpaired t-test.

Results

TFM-C inhibits cytokine secretion from activated U937 cells concomitant with induction of an ER stress response

In a recombinant cell system, TFM-C inhibits IL-12 secretion via a mechanism involving the induction of ER stress coupled to intracellular degradation of the cytokine polypeptide chains via the ER stress protein HERP [23,24,26]. In order to verify whether the cytokine secretion-inhibitory effect of TFM-C extends to natural cytokine producer cells, we assessed its effect using PMA/LPS-activated U937 macrophages, a well-known source of multiple cytokines. TFM-C potently blocked secretion of IL-β, IL-6, IL-8, IL-10, IL-12 and TNF-α (Figure 1A, C). By means of QPCR, TFM-C was found to suppress mRNA production of IL-10 over the course of the experiment, and at 12 and 24 h of TFM-C treatment, of IL-1β. Virtually no effect was seen on mRNA production of TNF-α and IL-8, while TFM-C increased IL-6 mRNA between 6 and 12 h. To verify whether TFM-C induced an ER stress response in U937 cells, we measured mRNA of HERP and IL-23p19, both of which have been associated with induction of ER stress [24,26,27]. This showed significant up-regulation of both genes by TFM-C while the housekeeping gene GAPDH was not affected (Figure 1D). Viability of U937 cells following exposure to TFM-C was assessed using two different methods (Figure 1B), and showed a limited percentage of apoptotic cells not exceeding 15 to 20% following 12 to 24 h of treatment. Thus, TFM-C blocks cytokine secretion in natural producer cells by ER stress-related mechanisms that may involve repressive effects on both cytokine mRNA production as well as on post-transcriptional and -translational events involved in cytokine secretion, such as the ER-retention

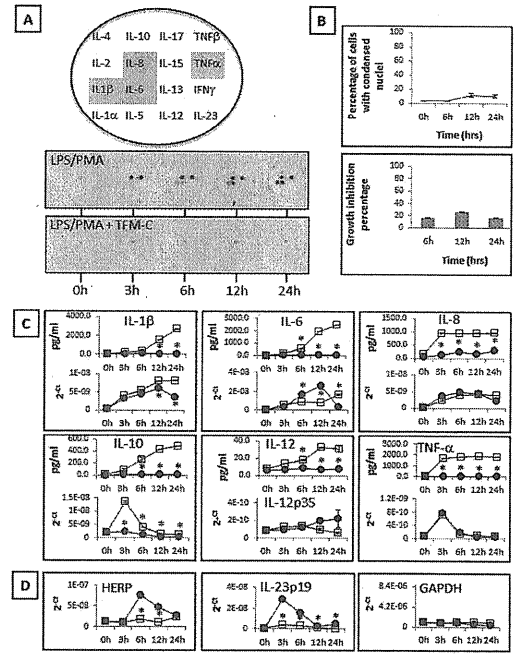

Figure 1 Effect of TFM-C on cytokine production from activated U937 macrophages. A. Lay-out of cytokine-specific antibody spots in the 16-plex cytokine Stripwell array (upper image) and visualization of cytokine-specific chemiluminescence in culture medium of LPS/PMA-treated U937 cells in the absence or presence of TFM-C (lower images). The grey-shaded cytokines in the upper images are those showing the highest production in LPS/PMA-treated U937 cells at 24 h. **B**. Effect of TFM-C treatment (50 μM) on the viability of macrophages (PMA-stimulated U937 cells). Apoptotic cells were measured by DAPI staining, and the percentage of damaged DNA and condensed chromatin was calculated following 6, 12 and 24 h of TFM-C treatment (upper graph). Metabolic activity of cells, measured by AlarmBlue®, was expressed as growth inhibition percentage of untreated controls for 6, 12 and 24 h of TFM-C treatment (lower graph). Bars show average of three independent experiments with corresponding error bars. **C**. Quantification of the kinetics of cytokine secretion and mRNA production (IL-1β, IL-6, IL-8, IL-10 IL-12 and TNF-α) in differentiated macrophages treated with LPS/PMA in the absence (open squares) or presence (solid circles) of TFM-C. All values represent the averages of three independent experiments. For each cytokine, the upper graph represents amount of secreted cytokine quantified using Quansys 16-plex Stripwells, while the lower graph represents cytokine-specific mRNA quantified by QPCR. Asterisks indicate significant differences at * $P < 0.05$ between TFM-C-treated and -untreated cells at each time point using Student's *t*-test. **D**. Effect of 50 μM TFM-C on IL-23p19, HERP and GAPDH mRNAs (QPCR) in differentiated macrophages, stimulated by LPS and PMA. The levels of mRNA levels are shown as 2^{-Ct}. Asterisks indicate significant differences at * $P < 0.05$ compared with baseline condition LPS/PMA-only using Student's *t*-test.

coupled to HERP-mediated degradation identified before for IL-12 [23,24,26]. However, of the TFM-C-sensitive cytokines identified in this experiment, IL-1β follows an unconventional protein secretion route involving

exocytosis of endolysosome-related vesicles not derived from the ER/Golgi system [28]. Given its blockage by TFM-C, which can not be explained by partial suppression of mRNA levels only, this indicates that TFM-C may suppress secretion of cytokines via interfering with both conventional ER-dependent and unconventional ER-independent transit routes.

TFM-C inhibits CIA

First, we examined the effect of TFM-C on CIA induced by immunizing DBA1/J mice with type II collagen. As shown in Figure 2A, administration of TFM-C strongly suppressed the severity of arthritis compared with vehicle-treated mice (*P*-value, < 0.05 by Mann-Whitney *U*-test compared with control from Day 26 and Day 36.). In contrast, administration of celecoxib showed only a mild suppressive effect on CIA, which is consistent with a previous report [19] (*P*-value, < 0.05 by Mann-Whitney *U*-test compared with control at Day 29 and Day 31.) In addition to visual scoring, we analyzed the histological features in the joints of four paws from TFM-C-, celecoxib- or vehicle-treated mice 37 days after disease induction. Quantification of the histological severity of arthritis is shown in Figure 2B and typical histological features are demonstrated in Figure 2C. Arthritis was not apparent in joints treated with TFM-C (Figure 2C, rightmost panel) compared to the severe arthritis with massive cell infiltration, cartilage erosion and bone destruction seen in joints of animals treated with vehicle (Figure 2C, leftmost panel). Both the clinical scores and pathological features of arthritis were significantly less severe in TFM-C-treated mice (Figure 2A-C). The pathological features, including cell infiltration and destruction of cartilage and bone, were slightly less severe in celecoxib-treated mice even though there is no statistically significant difference compared to vehicle-treated mice (Figure 2B). We next examined anti-CII antibody in TFM-C-, celecoxib- or vehicle-treated arthritic mice. There was a trend for reduction in both IgG1 and IgG2a isotypes as well as total IgG anti-CII in TFM-C-treated mice compared to vehicle-treated mice (Figure 2D), but the difference did not reach statistical significance. These results indicate that TFM-C possesses a potent inhibitory effect on CIA compared to vehicle or celecoxib. However, TFM-C treatment had little effect on CII-specific responses.

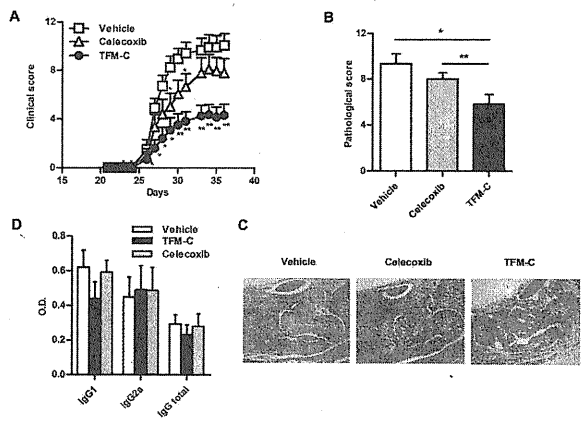

Figure 2 The effect of TFM-C on CIA. A. Clinical scores of CIA in DBA1/J mice treated with 10 μg/g TFM-C (closed circles), celecoxib (open triangles) or vehicle (open squares) every other day from 21 days after immunization. The data shown are pooled from two similar experiments. Error bars represent + SEM of 10 to 12 mice per group. * $P < 0.05$ compared with control group. * $P < 0.05$ compared with both control and celecoxib-treated groups. **B.** Quantification of histological assessment of joints 37 days after induction of CIA. Result shown is the mean + SEM of five mice per group. * $P < 0.05$, TFM-C-treated versus vehicle-treated group. * $P < 0.05$, celecoxib-treated versus TFM-C-treated group. **C.** Representative histological feature of joints in vehicle-treated (left), TFM-C-treated (right) and celecoxib-treated (middle) mice. (H&E stained; original magnification × 40). **D.** The effect of TFM-C on CII-specific response. CII-specific antibody responses in vehicle- (open bars), TFM-C- (filled bars) and celecoxib-treated (gray bars) group. Individual serum samples were obtained at Day 37 after the induction of arthritis and were analyzed as indicated in Materials and Methods. Data represent the mean + SEM of five mice per group.

TFM-C inhibits CAIA

Although TFM-C treatment suppressed clinical and pathological severities of CIA, CII-specific antibody levels were not reduced by TFM-C treatment. Therefore, we hypothesized that TFM-C treatment may have a strong inhibitory effect on the effector phase of arthritis. To test this hypothesis, we examined the effect of TFM-C on CAIA induced by injecting a mixture of monoclonal antibodies against type II collagen (CII) followed by lipopolysaccharide (LPS) administration two days later. The major players in CAIA are innate immune cells while adaptive immune cells are not required for disease development. Therefore, CAIA has value as an animal model to study the effector phase of arthritis. In vehicle-treated mice, severe arthritis occurred one week after CII antibody injection, and administration of celecoxib inhibited arthritis slightly (Figure 3A). In contrast, administration of TFM-C significantly suppressed CAIA compared to vehicle or celecoxib treatment. We next analyzed the histological features in the joints of four paws from vehicle-, TFM-C- and celecoxib-treated mice 12 days after disease induction. Quantification of the histological severity of arthritis is shown in Figure 3B and typical histological features are presented in Figure 3C. Massive cell infiltration, cartilage erosion, and bone destruction were observed in joints of vehicle-treated or celecoxib-treated mice but not in those of TFM-C-treated mice (Figure

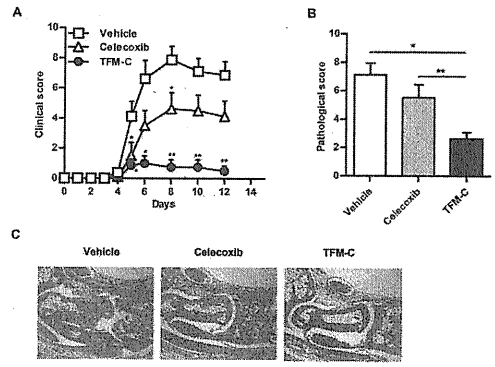

Figure 3 The effect of TFM-C on CAIA. A. Clinical scores of CAIA in B6 mice treated with 10 μg/g TFM-C (closed circles), celecoxib (open triangles) or vehicle (open squares) every other day from two days before CAIA induction. * $P < 0.05$ compared with control group, * $P < 0.05$ compared with both control and celecoxib-treated groups. Results shown are the mean + SEM of five mice per group. The data shown are from a single experiment representative of two similar experiments. **B.** Quantification of histological assessment of joints 12 days after induction of AIA shown in A. Results shown are the mean + SEM of five mice per group. * $P < 0.05$ control versus TFM-C group, * $P < 0.05$ celecoxib versus TFM-C -treated group. **C.** Representative histological feature of joints in vehicle-treated (left), TFM-C-treated (middle) and celecoxib-treated (right) mice. (H&E stained; original magnification × 40).

3B, C). These results indicate that TFM-C exhibits a strong disease inhibitory effect in CAIA in contrast to vehicle or celecoxib.

TFM-C inhibits the mast cell activation in CAIA

Next, we sought to understand the mechanism through which TFM-C treatment suppressed arthritis in CAIA. Since mast cells have been demonstrated to be critical for initiation of antibody-induced arthritis [29], we evaluated the effect of TFM-C on the activation of mast cells. Because degranulation is the clearest histological hallmark of mast cell activation, joint mast cells were visually assessed for an intact versus degranulating phenotype after staining with toluidine blue. The proportion of degranulated mast cells was significantly lower in TFM-C-treated mice compared to that in celecoxib- or vehicle-treated mice (Figure 4A, B).

TFM-C supresses the activation of macrophages

Innate immune cells and inflammatory cytokines, such as IL-1 and TNF-α are critical for disease development in CAIA [30]. Thus, we next determined the effect of TFM-C on the production of inflammatory cytokines from macrophages. Splenic macrophages from mice treated with TFM-C, celecoxib or control vehicle, were stimulated with LPS *ex vivo*, and the cytokines in the culture supernatants were measured by ELISA. The production of IL-1, IL-6 and TNF-α from macrophages was efficiently suppressed in TFM-C-treated mice compared to vehicle-treated mice (Figure 5). In celecoxib-treated mice, although the production of IL-1β was decreased, the production of other cytokines such as IL-6 and TNF-α was not suppressed, and the IL-6 production was even enhanced compared to vehicle-treated mice.

TFM-C suppresses leukocyte influx in thioglycollate-induced peritonitis

The other key players in antibody-induced arthritis are neutrophils [31-34]. Neutrophils are recruited to joint tissue and depletion of neutrophils has been shown to supress disease susceptibility and severity in CAIA [35]. An intraperitoneal injection of thioglycollate causes leukocytes influx into the peritoneum from bone marrow and circulation, and neutrophils are the major cell population which first emigrate to the peritoneal cavity. To assess the effect of TFM-C on neutrophil recruitment, mice were treated with TFM-C, celecoxib or control vehicle, and thioglycollate was injected intraperitoneally. Leukocyte cell numbers in the peritoneal cavity four hours after thioglycollate injection were comparable between control and celecoxib-treated groups (Figure 6). However, the peritoneal infiltrating cell numbers were reduced in mice treated with TFM-C, suggesting the suppressive effect of TFM-C on neutrophil recruitment.

Taken together, these results indicate that the activation of innate immune cells, including mast cells, macrophages, and neutrophils, is suppressed in TFM-C-treated mice but not in celecoxib-treated mice.

Discussion

In the present study we demonstrate, using arthritis models, that TFM-C, a celecoxib analogue with 205-fold lower COX-2-inhibitory activity, inhibits autoimmune disease. TFM-C differs from celecoxib by the substitution of the 4-methyl group by a trifluoromethyl group. This substitution drastically increases the IC_{50}s for inhibition of COX1 (15 μM to >100 μM for celecoxib and TFM-C, respectively) and COX2 (0.04 μM to 8.2 μM, respectively), but does not affect the apoptotic index measured in PC3 prostate cancer cells, indicating independence between structural requirements for COX-2 inhibition and apoptosis induction [36]. Celecoxib perturbs intracellular calcium by blocking ER Ca^{2+} ATPases, and this activity is shared with TFM-C [23,37]. In a HEK293 recombinant cell system, this Ca^{2+} perturbation is associated with inhibition of secretion and altered intracellular interaction of IL-12 polypeptide chains with the ER chaperones calreticulin and ERp44, and results in the interception of IL-12 by HERP

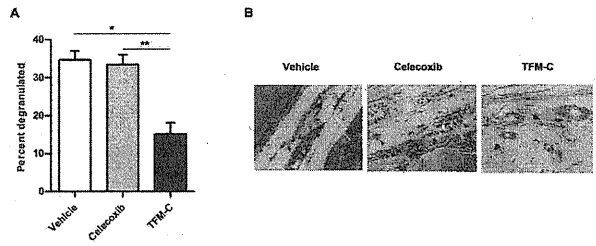

Figure 4 TFM-C inhibits the mast cell activation in CAIA. CAIA was induced in B6 mice and the mice were then treated with 10 μg/g TFM-C, celecoxib or vehicle as described in Figure 2. **A**. Quantification of degranulated mast cells in synovium of joints 12 days after induction of CAIA. * $P < 0.05$, compared with vehicle-treated group. * $P < 0.05$, compared with celecoxib-treated group. Results shown are the mean + SEM of six mice per group and were pooled from two experiments. **B**. Hisopathologic features of degranulated or intact mast cells in joints of representative vehicle-, celecoxib- and TFM-C- treated mice (toluidine blue stained; original magnification, × 100). White arrows indicate intact mast cells and black arrows indicate degranulated mast cells.

followed by degradation of the cytokine [23,24,26]. While IC_{50}s for inhibition of IL-12 secretion by celecoxib or TFM-C are similar [23,24], in the present paper, we show that TFM-C inhibits production of various cytokines from activated macrophages (Figures 1 and 5) and exerts a strikingly stronger inhibitory effect on arthritis models compared to celecoxib. Given that the main biological difference between celecoxib and TFM-C resides in the extent of COX-1 and -2 inhibition, it is, therefore, likely that the less potent effect of TFM-C on COX1/2 inactivation is a contributing, disease-limiting rather than disease-promoting factor in these arthritis models. Indications supporting this concept come from a study showing increased LPS-induced macrophage production of TNF-α by inactivation of COX-2 with celecoxib [38]. Up-regulation of TNF-α by celecoxib was also reported in human PBMCs, rheumatoid synovial cultures and whole blood [20]. The relation between the anticipated extent of COX inhibition and production of TNF-α was observed in the present study (Figure 5), where activated macrophages showed a tendency toward increased or decreased TNF-α production in the presence of celecoxib or TFM-C, respectively, compared to vehicle-treated cells. In this cell system (Figure 5), celecoxib significantly increased production of the pro-inflammatory cytokine IL-6 while TFM-C suppressed it. Pending future mechanistic studies, this data indicate that prostaglandin-mediated suppressive effects, or other, as yet to be identified differential TFM-C/celecoxib-related effects on TNF-α production may extend to other cytokines as well, and provide an important clue as to the more potent beneficial effects of TFM-C compared to celecoxib in the arthritis models presented here.

The suppression of antibody-induced arthritis, which requires innate but not acquired immune cells [29-34,39], suggests that TFM-C also inhibits the activation of innate immune cells while celecoxib does not. In fact, TFM-C suppresses the production of inflammatory cytokines from macrophages and the activation of mast cells as well as the subsequent recruitment of leukocytes. Mast cells are essential for the initiation of antibody-induced arthritis [29]. Moreover, mast cells are present in human synovia [40-43] and are an important

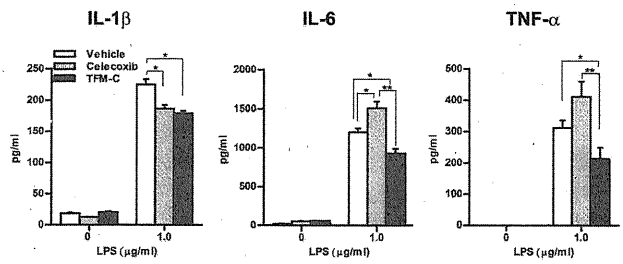

Figure 5 TFM-C supresses the activation of macrophages. B6 mice recieved 10 μg/g TFM-C, celecoxib or vehicle on Day 0 and Day 2, and on Day 3, splenic macrophages were collected and were stimulated by LPS *in vitro* in the presence of TFM-C, celecoxib or vehicle. Cytokines were detected by ELISA. IL-1β and IL-6 were measured 24 h after stimulation. TNF-α was measured six hours after stimulation. The data shown are from a single experiment representative of three similar experiments. * $P < 0.05$ compared with control group, * $P < 0.05$ compared with celecoxib-treated group.

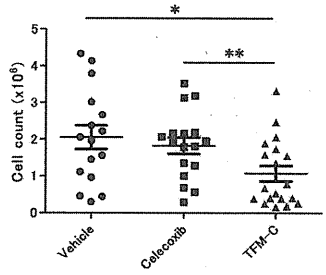

Figure 6 TFM-C supresses leukocyte influx in thioglycollate-induced peritonitis. B6 mice recieved 10 μg/g TFM-C, celecoxib or vehicle at two days and one hour before peritoneal injection of thioglycollate. At four hours after thioglycollate injection, peritoneal lavage fluid was collected and the infiltrating cells were counted. Cell numbers are shown from three separate experiments. * $P < 0.05$, TFM-C-treated versus vehicle-treated group. * $P < 0.05$, celecoxib-treated versus TFM-C-treated group.

source of both proteases and inflammatory cytokines, including IL-17, in patients with rheumatoid arthritis [42-44]. The clear difference between the effects of TFM-C and celecoxib on the suppression of mast cell activation could explain the differential impact of these compounds on arthritis models. Mast cells are important not only in arthritis but also in other conditions, such as allergy, obesity and diabetes [45]. Therefore, the suppression of mast cell activation by TFM-C may be applicable for the inhibition of these diseases in addition to autoimmune diseases.

Cytokines and chemokines, such as TNF-α and MCP-1, produced by macrophages, are suggested to play important roles for neutrophil influx in thioglycollate-induced peritonitis [46]. Mast cells were shown to produce TNF-α, which recruits neutrophils into the peritoneum in an immune complex peritonitis model [47]. Thus, it is likely that TFM-C suppressed macrophages and mast cells produce such chemoattractants, which in turn inhibited neutrophil influx into the peritoneum. However, it is also possible that TFM-C directly suppressed neutrophil activation. Further studies are required to address this possibility.

As described above, the major players in CAIA are innate immune cells, while adaptive immune cells are not required for disease development. Therefore, CAIA has value as an animal model for the study of the effector phase of arthritis. However, it is well known that adaptive immune cells play a significant role in the pathogenesis of RA and the strongest genetic link in RA is the association with HLA-DR, which is thought to present autoantigens to T cells. The activation of T cells and B cells is believed to initiate and/or enhance the effector inflammation phase of arthritis. In fact, massive infiltration of T and B cells is observed in RA synovium. Therefore, the ideal therapeutic agents for RA are those displaying the capacity to suppress both the induction and effector phases of arthritis. TFM-C treatment suppresses CIA, which requires both innate and adaptive immune cells for the development of arthritis. We previously demonstrated that celecoxib treatment suppresses EAE induced by immunizing B6 mice with myelin oligodendrocyte glycoprotein$_{35-55}$ (MOG) peptide [22]. The suppression of EAE by celecoxib was COX-2 independent and was accompanied by reduced IFN-γ production by MOG-reactive T cells. We observed a trend of reduced anti-CII antibody levels in serum upon TFM-C treatment. As TFM-C inhibited secretion of both recombinant IL-12 and IL-23 using a pIND ponasterone-inducible vector system in HEK293 cells [23,24], TFM-C treatment may have also influenced CII-specific immune responses by suppressing antigen-presenting cells.

Specific inhibition of COX-2 has some adverse effects. Rofecoxib, a highly specific COX-2 inhibitor, was withdrawn from the world market because of an increased rate of cardiovascular events in patients with colorectal polyps [48]. Celecoxib was also shown to augment cardiovascular and thrombotic risk in colorectal adenoma patients, especially in the subgroup suffering from pre-existing atherosclerotic heart disease [49]. Moreover, inhibition of COX-2 activity has been reported to exacerbate brain inflammation by increasing glial cell activation [50]. It has been suggested that the inhibition of COX-2-dependent prostaglandin I_2 from endothelial cells may be the major cause of thrombosis [51]. As the COX-2-inhibitory activity of TFM-C is 205-fold lower than that of celecoxib, the arthritis suppression by TFM-C appears to be independent of COX-2 inhibition. Therefore, TFM-C, which has strong immunoregulatory abilities but low COX-2-inhibitory activity, could serve as a new disease-modifying agent to prevent the progression of autoimmune diseases such as RA.

Conclusions

In summary, TFM-C, a trifluoromethyl analogue of celecoxib, inhibits arthritis despite the fact that TFM-C possesses very low COX-2-inhibitory activity. The most striking features of TFM-C are its inhibitory effect on the activation of innate immune cells and its suppression of arthritis compared to celecoxib. TFM-C treatment suppressed both CIA and CAIA by targeting innate immune cells, which are involved in both the induction and the effector phases of arthritis inflammation. Taking these data together, TFM-C may serve as an effective therapeutic drug for arthritis, including RA.

Abbreviations

B6: C57BL/6J; CII: anti-type II collagen; CAIA: type II collagen antibody-induced arthritis; CFA: complete Freund's adjuvant; CIA: collagen-induced arthritis; COX-2: cycloooxygenase-2; EAE: experimental autoimmune

encephalomyelitis; ELISA: enzyme-linked immunosorbent assay; IFA: incomplete Freund's adjuvant; IL: interleukin; LPS: lipopolysaccharide; MOG: myelin oligodendrocyte glycoprotein; *Mtb*: *Mycobacterium tuberculosis*; PBS: phosphate-buffered saline; TFM-C: a trifluoromethyl analogue of celecoxib; TNF: tumor necrosis factor.

Acknowledgements
This work was supported by Japan Foundation for Neuroscience and Mental Health (AC), a Grant-in-Aid for Scientific Research (B: 7210 to SM) from the Japan Society for the Promotion of Science, and Health and Labour Sciences Research Grants on Intractable Diseases (Neuroimmunological Diseases) from the Minitry of Health, Labour and Welfare of Japan; and by grants to KV from the Ministerio de Ciencia e Innovación, Madrid, Spain (MEC-2008; SAF2008-00433) and from the Gobierno Vasco's SAIOTEK Program (Ref. S-PE09UN33).

Author details
[1]Department of Immunology, National Institute of Neuroscience, National Center of Neurology and Psychiatry, 4-1-1 Ogawahigashi, Kodaira, Tokyo 187-8502, Japan. [2]Neurogenomiks Laboratory, Universidad Del País Vasco (UPV/EHU), Parque Tecnológico de Bizkaia, 48170 Zamudio, Spain. [3]IKERBASQUE, Basque Foundation for Science, 48011, Bilbao, Spain.

Authors' contributions
AC, MM, CT, RT and AP performed and evaluated experiments. AC, TY, KV and SM designed and supervised the experiments. IA and KV provided TFM-C. AC, KV and SM prepared the manuscript. All authors have read and approved the manuscript for publication.

Competing interests
The authors declare that they have no competing interests.

Received: 14 June 2011 Revised: 13 December 2011
Accepted: 17 January 2012 Published: 17 January 2012

References

1. Krieckaert CL, Bartelds GM, Lems WF, Wolbink GJ: **The effect of immunomodulators on the immunogenicity of TNF-blocking therapeutic monoclonal antibodies: a review.** *Arthritis Res Ther* 2010, **12**:217.
2. Feldmann M, Maini SR: **Role of cytokines in rheumatoid arthritis: an education in pathophysiology and therapeutics.** *Immunol Rev* 2008, **223**:7-19.
3. Buch MH: **Sequential use of biologic therapy in rheumatoid arthritis.** *Curr Opin Rheumatol* 2010, **22**:321-329.
4. Nishimoto N, Yoshizaki K, Miyasaka N, Yamamoto K, Kawai S, Takeuchi T, Hashimoto J, Azuma J, Kishimoto T: **Treatment of rheumatoid arthritis with humanized anti-interleukin-6 receptor antibody: a multicenter, double-blind, placebo-controlled trial.** *Arthritis Rheum* 2004, **50**:1761-1769.
5. Maini RN, Taylor PC, Szechinski J, Pavelka K, Bröll J, Balint G, Emery P, Raemen F, Petersen J, Smolen J, Thomson D, Kishimoto T, CHARISMA Study Group: **Double-blind randomized controlled clinical trial of the interleukin-6 receptor antagonist, tocilizumab, in European patients with rheumatoid arthritis who had an incomplete response to methotrexate.** *Arthritis Rheum* 2006, **54**:2817-2829.
6. Genovese MC, McKay JD, Nasonov EL, Mysler EF, da Silva NA, Alecock E, Woodworth T, Gomez-Reino JJ: **Interleukin-6 receptor inhibition with tocilizumab reduces disease activity in rheumatoid arthritis with inadequate response to disease-modifying antirheumatic drugs: the tocilizumab in combination with traditional disease-modifying antirheumatic drug therapy study.** *Arthritis Rheum* 2008, **58**:2968-2980.
7. Smolen JS, Beaulieu A, Rubbert-Roth A, Ramos-Remus C, Rovensky J, Alecock E, Woodworth T, Alten R, OPTION Investigators: **Effect of interleukin-6 receptor inhibition with tocilizumab in patients with rheumatoid arthritis (OPTION study): a double-blind, placebo-controlled, randomized trial.** *Lancet* 2008, **371**:987-997.
8. Emery P, Fleischmann R, Filipowicz-Sosnowska A, Schechtman J, Szczepanski L, Kavanaugh A, Racewicz AJ, van Vollenhoven RF, Li NF, Agarwal S, Hessey EW, Shaw TM, DANCER Study Group: **The efficacy and safety of rituximab in patients with active rheumatoid arthritis despite methotrexate treatment: results of a phase IIB randomized, double-blind, placebo-controlled, dose-ranging trial.** *Arthritis Rheum* 2006, **54**:1390-1400.
9. Cohen SB, Emery P, Greenwald MW, Dougados M, Furie RA, Genovese MC, Keystone EC, Loveless JE, Burmester GR, Cravets MW, Hessey EW, Shaw T, Totoritis MC, REFLEX Trial Group: **Rituximab for rheumatoid arthritis refractory to anti-tumor necrosis factor therapy: results of a multicenter, randomized, double-blind, placebo-controlled, phase III trial evaluating primary efficacy and safety at twenty-four weeks.** *Arthritis Rheum* 2006, **54**:2793-2806.
10. Kremer JM, Westhovens R, Leon M, Di Giorgio E, Alten R, Steinfeld S, Russell A, Dougados M, Emery P, Nuamah IF, Williams GR, Becker JC, Hagerty DT, Moreland LW: **Treatment of rheumatoid arthritis by selective inhibition of T-cell activation with fusion protein CTLA4Ig.** *N Engl J Med* 2003, **349**:1907-1915.
11. Lopez-Diego RS, Weiner HL: **Novel therapeutic strategies for multiple sclerosis-a multifaceted adversary.** *Nat Rev Drug Discov* 2008, **7**:909-925.
12. Yazici Y: **Treatment of rheumatoid arthritis: we are getting there.** *Lancet* 2009, **374**:178-180.
13. Myers LK, Kang AH, Postlethwaite AE, Rosloniec EF, Morham SG, Shlopov BV, Goorha S, Ballou LR: **The genetic ablation of cyclooxygenase 2 prevents the development of autoimmune arthritis.** *Arthritis Rheum* 2000, **43**:2687-2693.
14. Trebino CE, Stock JL, Gibbons CP, Naiman BM, Wachtmann TS, Umland JP, Pandher K, Lapointe JM, Saha S, Roach ML, Carter D, Thomas NA, Durtschi BA, McNeish JD, Hambor JE, Jakobsson PJ, Carty TJ, Perez JR, Audoly LP: **Impaired inflammatory and pain responses in mice lacking an inducible prostaglandin E synthase.** *Proc Natl Acad Sci USA* 2003, **100**:9044-9049.
15. Honda T, Segi-Nishida E, Miyachi Y, Narumiya S: **Prostacyclin-IP signaling and prostaglandin E2-EP2/EP4 signaling both mediate joint inflammation in mouse collagen-induced arthritis.** *J Exp Med* 2006, **203**:325-335.
16. Noguchi M, Kimoto A, Kobayashi S, Yoshino T, Miyata K, Sasamata M: **Effect of celecoxib, a cyclooxygenase-2 inhibitor, on the pathophysiology of adjuvant arthritis in rat.** *Eur J Pharmacol* 2005, **513**:229-235.
17. Tsuboi H, Nampei A, Matsui Y, Hashimoto J, Kawai S, Ochi T, Yoshikawa H: **Celecoxib prevents juxta-articular osteopenia and growth plate destruction adjacent to inflamed joints in rats with collagen-induced arthritis.** *Mod Rheumatol* 2007, **17**:115-122.
18. Taketa T, Sakai A, Tanaka S, Nakai K, Menuki K, Yamane H, Tanaka K, Nakamura T: **Selective cyclooxygenase-2 inhibitor prevents reduction of trabecular bone mass in collagen-induced arthritic mice in association with suppression of RANKL/OPG ratio and IL-6 mRNA expression in synovial tissues but not in bone marrow cells.** *J Bone Miner Metab* 2008, **26**:143-151.
19. Anderson GD, Keys KL, De Ciechi PA, Masferrer JL: **Combination therapies that inhibit cyclooxygenase-2 and leukotriene synthesis prevent disease in murine collagen induced arthritis.** *Inflamm Res* 2009, **58**:109-117.
20. Page TH, Turner JJ, Brown AC, Timms EM, Inglis JJ, Brennan FM, Foxwell BM, Ray KP, Feldmann M: **Nonsteroidal anti-inflammatory drugs increase TNF production in rheumatoid synovial membrane cultures and whole blood.** *J Immunol* 2010, **185**:3694-3701.
21. Grosch S, Tegeder I, Niederberger E, Brautigam L, Geisslinger G: **COX-2 independent induction of cell cycle arrest and apoptosis in colon cancer cells by the selective COX-2 inhibitor celecoxib.** *FASEB J* 2001, **15**:2742-2744.
22. Miyamoto K, Miyake S, Mizuno M, Oka N, Kusunoki S, Yamamura T: **Selective COX-2-inhibitor celecoxib prevents experimental autoimmune encephalomyelitis through COX-2-independent pathway.** *Brain* 2006, **129**:1984-1992.
23. Alloza I, Baxter A, Chen Q, Matthiesen R, Vandenbroeck K: **Celecoxib inhibits interleukin-12 alphabeta and beta2 folding and secretion by a novel COX2-independent mechanism involving chaperones of the endoplasmic reticulum.** *Mol Pharmacol* 2006, **69**:1579-1587.
24. McLaughlin M, Alloza I, Quoc HP, Scott CJ, Hirabayashi Y, Vandenbroeck K: **Inhibition of secretion of interleukin (IL)-12/23 family cytokines by 4-trifluoromethyl-celecoxib is coupled to degradation via the endoplasmic reticulum stress protein HERP.** *J Biol Chem* 2010, **285**:6960-6969.
25. Kaieda S, Tomi C, Oki S, Yamamura T, Miyake S: **Activation of invariant natural killer T cells by synthetic glycolipid ligands suppresses autoantigody-induced arthritis.** *Arthritis Rheum* 2007, **56**:1836-1845.

26. McLaughlin M, Vandenbroeck K: **The endoplasmic reticulum protein folding factory and its chaperones: new targets for drug discovery?** *Br J Pharmacol* 2011, **162**:328-345.
27. Wheeler MC, Rizzi M, Sasik R, Almanza G, Hardiman G, Zanetti M: **KDEL-retained antigen in B lymphocytes induces a proinflammatory response: a posible role for endoplasmic reticulum stress in adaptive T cell immunity.** *J Immunol* 2008, **181**:256-264.
28. Andrei C, Dazzi C, Lotti L, Torrisi MR, Chimini G, Rubartelli A: **The secretory route of the leaderless protein interleukin 1beta involves exocytosis of endolysosome-related vesicles.** *Mol Biol Cell* 1999, **10**:1463-1475.
29. Lee DM, Friend DS, Gurish MF, Benoist C, Mathis D, Brenner MB: **Mast cells: a cellular link between autoantibodies and inflammatory arthritis.** *Science* 2002, **297**:1689-1692.
30. Kagari T, Doi H, Shimozato T: **The importance of IL-1 beta and TNF-alpha, and the noninvolvement of IL-6, in the development of monoclonal antibody-induced arthritis.** *J Immunol* 2002, **169**:1459-1466.
31. Chen M, Lam BK, Kanaoka Y, Nigrovic PA, Audoly LP, Austen KF, Lee DM: **Neutrophil-derived leukotriene B4 is required for inflammatory arthritis.** *J Exp Med* 2006, **203**:837-842.
32. Kim ND, Chou RC, Seung E, Tager AM, Luster AD: **A unique requirement for the leukotriene B4 receptor BLT1 for neutrophil recruitment in inflammatory arthritis.** *J Exp Med* 2006, **203**:829-835.
33. Zhou JS, Xing W, Friend DS, Austen KF, Katz HR: **Mast cell deficiency in Kit (W-sh) mice does not impair antibody-mediated arthritis.** *J Exp Med* 2007, **204**:2797-802.
34. Chou RC, Kim ND, Sadik CD, Seung E, Lan Y, Byme MH, Haribabu B, Iwakura Y, Luster AD: **Lipid-cytokine-chemokine cascade drives neutrophil recruitment in a murine model of inflammatory arthritis.** *Immunity* 2010, **33**:266-278.
35. Nandakumar KS, Svensson L, Holmdahl R: **Collagen type II-specific monoclonal antibody-induced arthritis in mice: description of the disease and the influence of age, sex, and genes.** *Am J Pathol* 2003, **163**:1827-1837.
36. Zhu J, Song X, Lin HP, Young DC, Yan S, Marquez VE, Chen CS: **Using cyclooxygenase-2 inhibitors as molecular platforms to develop a new class of apoptosis-inducing agents.** *J Natl Cancer Inst* 2002, **94**:1745-1757.
37. Johnson AJ, Hsu AL, Lin HP, Song X, Chen CS: **The cyclo-oxygenase-2 inhibitor celecoxib perturbs intracellular calcium by inhibiting endoplasmic reticulum Ca2+-ATPases: a plausible link with its anti-tumour effect and cardiovascular risks.** *Biochem J* 2002, **366**:831-837.
38. Gitlin JM, Loftin CD: **Cyclooxygenase-2 inhibition increases lipopolysaccharide-induced atherosclerosis in mice.** *Cardiovasc Res* 2009, **81**:400-407.
39. Wipke BT, Allen PM: **Essential role of neutrophils in the initiation and progression of a murine model of rheumatoid arthritis.** *J Immunol* 2010, **167**:1601-1608.
40. Bromley M, Fisher WD, Woolley DE: **Mast cells at sites of cartilage erosion in the rheumatoid joint.** *Ann Rheum Dis* 1984, **43**:76-79.
41. Kiener HP, Baghestanian M, Dominkus M, Walchshofer S, Ghannadan M, Willheim M, Sillaber C, Graninger WB, Smolen JS, Valent P: **Expression of the C5a receptor (CD88) on synovial mast cells in patients with rheumatoid arthritis.** *Arthritis Rheum* 1998, **41**:233-245.
42. Sawamukai N, Yukawa S, Saito K, Nakayamada S, Kambayashi T, Tanaka Y: **Mast cell-derived tryptase inhibits apoptosis of human rheumatoid synovial fibroblasts via rho-mediated signaling.** *Arthritis Rheum* 2010, **62**:952-959.
43. Eklund KK: **Mast cells in the pathogenesis of rheumatic diseases and as potential targets for anti-rheumatic therapy.** *Immunol Rev* 2007, **217**:38-52.
44. Hueber AJ, Asquith DL, Miller AM, Reilly J, Kerr S, Leipe J, Melendez AJ, McInnes IB: **Mast cells express IL-17A in rheumatoid arthritis synovium.** *J Immunol* 2010, **184**:3336-3340.
45. Liu J, Divoux A, Sun J, Zhang J, Clement K, Glickman JN, Sukhova GK, Wolters PJ, Du J, Gorgun CZ, Doria A, Libby P, Blumberg RS, Kahn BB, Hotamisligil GS, Shi GP: **Genetic deficiency and pharmacological stabilization of mast cells reduce diet-induced obesity and diabetes in mice.** *Nat Med* 2009, **15**:940-945.
46. Matsukawa A, Kudo S, Maeda T, Numata K, Watanabe H, Takeda K, Akira S, Ito T: **Stat3 in resident macrophages are a repressor protein of inflammatory response.** *J Immunol* 2005, **175**:3354-3359.
47. Zhang Y, Ramos BF, Jakschik BA: **Neutrophil recruitment by tumor necrosis factor from mast cells in immune complex peritonitis.** *Science 192* **258**:1957-1959.
48. Bresalier RS, Sandler RS, Quan H, Bolognese JA, Oxenius B, Horgan K, Lines C, Riddell R, Morton D, Lanas A, Konstam MA, Baron JA: **Adenomatous Polyp Prevention on Vioxx (APPROVe) Trial Investigators. Cardiovascular events associated with rofecoxib in a colorectal adenoma chemoprevention trial.** *N Eng J Med* 2005, **352**:1092-1102.
49. Bertagnolli MM, Eagle CJ, Zauber AG, Redston M, Breazna A, Kim K, Tang J, Rosenstein RB, Umar A, Bagheri D, Collins NT, Burn J, Chung DC, Dewar T, Foley TR, Hoffman N, Macrae F, Pruitt RE, Saltzman JR, Salzberg B, Sylwestrowicz T, Hawk ET, Adenoma Prevention with Celecoxib Study Investigators: **Five-year efficacy and safety analysis of the adenoma prevention with celecoxib trial.** *Cancer Prev Res (Phila)* 2009, **2**:310-321.
50. Aid S, Langenbach R, Bosetti F: **Neuroinflammatory response to lipopolysaccharide is exacerbated in mice genetically deficient in cyclooxygenase-2.** *J Neuroinflammation* 2008, **5**:17-30.
51. Kobayashi T, Tahara Y, Matsumoto M, Iguchi M, Sano H, Murayama T, Arai H, Oida H, Yurugi-Kobayashi T, Yamashita JK, Katagiri H, Majima M, Yokode M, Kita T, Narumiya S: **Roles of thromboxane A(2) and prostacyclin in the development of atherosclerosis in apoE-deficient mice.** *J Clin Invest* 2004, **114**:784-794.

doi:10.1186/ar3683
Cite this article as: Chiba *et al.*: A 4-trifluoromethyl analogue of celecoxib inhibits arthritis by suppressing innate immune cell activation. *Arthritis Research & Therapy* 2012 **14**:R9.

Interleukin 6 signaling promotes anti-aquaporin 4 autoantibody production from plasmablasts in neuromyelitis optica

Norio Chihara[a,b], Toshimasa Aranami[a,c], Wakiro Sato[a], Yusei Miyazaki[a], Sachiko Miyake[a,c], Tomoko Okamoto[c,d], Masafumi Ogawa[c,d], Tatsushi Toda[b], and Takashi Yamamura[a,c,1]

[a]Department of Immunology, National Institute of Neuroscience, National Center of Neurology and Psychiatry (NCNP), Tokyo 187-8502, Japan; [b]Department of Neurology, Kobe University Graduate School of Medicine, Kobe 650-0017, Japan; and [c]Multiple Sclerosis Center and [d]Department of Neurology, National Center Hospital, NCNP, Tokyo 187-8551, Japan

Edited* by Tadamitsu Kishimoto, Graduate School of Frontier Biosciences, Osaka University, Suita, Japan, and approved January 26, 2011 (received for review November 21, 2010)

Neuromyelitis optica (NMO) is an inflammatory disease affecting the optic nerve and spinal cord, in which autoantibodies against aquaporin 4 (AQP4) water channel protein probably play a pathogenic role. Here we show that a B-cell subpopulation, exhibiting the $CD19^{int}CD27^{high}CD38^{high}CD180^{-}$ phenotype, is selectively increased in the peripheral blood of NMO patients and that anti-AQP4 antibodies (AQP4-Abs) are mainly produced by these cells in the blood of these patients. These B cells showed the morphological as well as the phenotypical characteristics of plasmablasts (PB) and were further expanded during NMO relapse. We also demonstrate that interleukin 6 (IL-6), shown to be increased in NMO, enhanced the survival of PB as well as their AQP4-Ab secretion, whereas the blockade of IL-6 receptor (IL-6R) signaling by anti–IL-6R antibody reduced the survival of PB in vitro. These results indicate that the IL-6–dependent B-cell subpopulation is involved in the pathogenesis of NMO, thereby providing a therapeutic strategy for targeting IL-6R signaling.

neuroinflamatory disease | autoimmunity | multiple sclerosis | central nervous system | IL-6 receptor blockade

Neuromyelitis optica (NMO) is an inflammatory demyelinating disorder characterized by recurrent attacks of severe optic neuritis and myelitis. Unlike the conventional form of multiple sclerosis (CMS), the lesions of NMO tend to spare the cerebral white matter, especially during the early stage (1), and even a single episode of attack can cause serious neurological deficits such as total blindness and paraplegia. Accordingly, accumulation of irreversible damage to the central nervous system (CNS) along with rapid progression of disability is more frequently found in NMO compared with CMS (2).

NMO can be distinguished from CMS by clinical, neuroimaging, and serological criteria (3). It is now known that serum anti-aquaporin 4 (AQP4) autoantibodies can be used as a disease marker of NMO (1, 2). AQP4 is the most abundantly expressed water channel protein in the CNS and is highly expressed in the perimicrovessel astrocyte foot processes, glia limitans, and ependyma (4). Emerging clinical and pathological observations suggest that anti-AQP4 antibodies (AQP4-Abs) play a key role in the pathogenesis of NMO. Prior studies have documented a significant correlation of serum AQP4-Ab levels with the therapeutic efficacy of plasma exchange during clinical exacerbations of NMO (2, 5). In the CNS lesions of NMO, reduced expression of AQP4 on astrocytes is evident even during the early stage (6), which is followed by the occurrence of vasculocentric destruction of astrocytes associated with perivascular deposition of complement and IgG (7).

On the other hand, recent studies have suggested that AQP4-Abs alone are incapable of causing the clinical and pathological features of NMO. In fact, Hinson et al. emphasized the role of cellular immunity in combination with AQP4-Abs by showing that the attack severity of NMO was not correlated with serum AQP4-Ab levels (8). It was also demonstrated that direct injection of IgGs derived from NMO patients into the brains of naïve mice did not cause NMO-like lesions, although brain tissue destruction associated with leukocyte infiltration was elicited by coinjecting human complement (9). Other groups have shown that the passive transfer of IgGs from NMO patients to rats challenged with induction of experimental autoimmune encephalomyelitis (EAE) may cause a decrease in the expression of AQP4 in astrocytes along with worsening of clinical EAE (10–12). In contrast, the transfer of IgGs to unimmunized rats did not cause any pathology. These results suggest that induction of AQP4-Ab–mediated pathology in NMO depends on the presence of complement, leukocytes, and T cells.

Although AQP4-Ab–secreting cells are a potential target for therapy, detailed characteristics of AQP4-Ab–producing cells have not been clarified yet. Because some NMO patients have elevated serum anti-nuclear and anti–SS-A/SS-B Abs (1), as found in patients with systemic lupus erythematosus (SLE) or Sjögren syndrome, NMO might share common pathological mechanisms with these autoimmune diseases. Kikuchi et al. previously reported that $CD180^{-}$ B cells are activated B cells capable of producing autoantibodies in SLE (13). CD180 is a member of the leucine-rich repeat family of molecules with homology to Toll-like receptor 4 (14), which is highly expressed by naïve and memory B cells but not by plasma cells (15). Odendahl et al. demonstrated that $CD27^{high}CD38^{+}$ B cells, capable of producing high-affinity IgG (16), are increased in the peripheral blood of SLE patients with some correlation to disease activity (17). Considering the phenotypes of autoantibody-producing cells reported in SLE, we analyzed the expression of CD27, CD38, and CD180 on $CD19^{+}$ B cells in the peripheral blood of NMO patients. We found that $CD27^{high}CD38^{high}CD180^{-}$ B cells were significantly increased in AQP4-Ab seropositive patients diagnosed with NMO or NMO spectrum disorder (1) compared with healthy subjects (HS) or CMS patients. Notably, this B-cell subpopulation was found to be a major source of AQP4-Abs in the peripheral blood of AQP4-Ab seropositive patients and depended on interleukin-6 receptor (IL-6R) signaling for survival.

Author contributions: N.C., T.A., S.M., and T.Y. designed research; N.C. and W.S. performed research; Y.M. and S.M. contributed new reagents/analytic tools; N.C., T.A., T.O., M.O., T.T., and T.Y. analyzed data; T.Y. supervised the work; and N.C., T.A., and T.Y. wrote the paper.

The authors declare no conflict of interest.

*This Direct Submission article had a prearranged editor.

Freely available online through the PNAS open access option.

[1]To whom correspondence should be addressed. E-mail: yamamura@ncnp.go.jp.

This article contains supporting information online at www.pnas.org/lookup/suppl/doi:10.1073/pnas.1017385108/-/DCSupplemental.

Results

$CD27^{high}CD38^{high}CD180^{-}$ B Cells Were Increased in the Peripheral Blood of NMO Patients. Although AQP4-Abs are identified as IgGs (18), no prior study has focused on proportional changes of B-cell subsets in NMO. We therefore performed multicolor flow cytometric analysis of peripheral blood mononuclear cells (PBMC) derived from patients and controls. After starting the study, we soon noticed a remarkable expansion of a distinct B-cell subset in some patients with NMO. The expanded B cells were identified as a population of $CD27^{high}$, $CD38^{high}$, and $CD180^{-}$, and showed lower expression of CD19 than other B cells (Fig. 1*A*). Notably, this population did not express the B-cell marker CD20 (Fig. S1). First, we collected samples from patients in remission and analyzed the pooled data. We found that the proportion of this subpopulation among $CD19^{+}$ B cells was significantly increased in AQP4-Ab seropositive patients with NMO or NMO spectrum disorder (Fig. 1*B*) compared with HS or CMS patients. There was no significant difference in the proportion of this B-cell subpopulation between those with typical NMO and those with NMO spectrum disorder. Furthermore, the frequency of this B-cell subpopulation was correlated with the serum AQP4-Ab titer (Fig. S2). Comparison of paired samples obtained from the same patients during relapse and in remission showed that the $CD27^{high}CD38^{high}CD180^{-}$ B cells further increased during relapse (Fig. 1*C*). In contrast, the frequencies of $CD27^{-}$ naïve B cells (nB) and $CD27^{+}CD38^{-low}$ memory B cells (mB) were not altered in AQP4-Ab seropositive patients compared with controls (Fig. S3). The large majority of seropositive patients were treated with corticosteroids. However, the frequency of $CD27^{high}CD38^{high}CD180^{-}$ cells among $CD19^{+}$ B cells was not correlated with the daily corticosteroid dose given to patients (Fig. S4). Moreover, the increase in cells in NMO patients was still evident compared with that in CMS patients similarly treated with corticosteroids (Fig. S5). Taken together, the selective increase in $CD27^{high}CD38^{high}CD180^{-}$ B cells in seropositive patients was thought to reflect their role in the pathogenesis of NMO but not to be an effect of the corticosteroid treatment.

Expanded Cells Resemble Early Plasma Cells in Gene Expression and Morphology. To gain insights into the developmental stage of the $CD27^{high}CD38^{high}CD180^{-}$ B cells, we quantified the mRNA expression of B-cell–associated transcription factors in sorted cell populations. Compared with nB and mB, this population showed much higher expression of B-lymphocyte-induced maturation protein 1 (Blimp-1) and IFN regulatory factor 4 (IRF4), which are essential for the regulation of plasma cell differentiation (19, 20) (Fig. 2*A*). In contrast, the expression of paired box gene 5 (PAX5), known to be down-regulated in early plasma cell differentiation (21), was reciprocally reduced in the B-cell subset. This gene expression pattern is very similar to that of plasma cells. However, it was notable that the cells of interest expressed CD19, which is not detected in mature plasma cells. Moreover, only 40% of this population expressed the most reliable plasma cell marker CD138 (22). Morphological analysis also confirmed the similarity of this population to plasma cells: they exhibit eccentric nucleus, perinuclear hof region, and abundant cytoplasm. However, they possess a larger nucleus with a lower extent of chromatin clumping compared with $CD138^{+}$ plasma cells derived from HS (Fig. 2*B*). Notably, the $CD138^{+}$ population among $CD27^{high}CD38^{high}CD180^{-}$ cells in NMO patients was

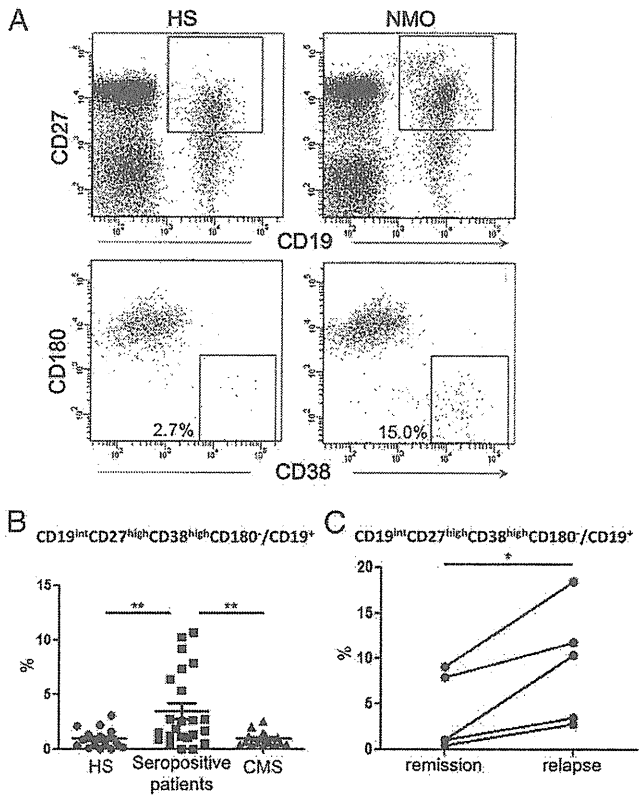

Fig. 1. $CD27^{high}CD38^{high}CD180^{-}$ B cells increased in NMO patients. (*A*) A flow cytometric scheme for the analysis of B-cell subpopulations. PBMC from HS and NMO in remission were stained with fluorescence-conjugated anti-CD19, -CD27, -CD38, and -CD180 mAbs. $CD19^{+}CD27^{+}$ cells were partitioned (*Upper*) and analyzed for expression of CD38 and CD180 (*Lower*). Values represent the percentage of $CD38^{high}CD180^{-}$ cells within $CD19^{+}CD27^{+}$ cells. (*B*) Analysis of the pooled data derived from patients in clinical remission. This shows the percentages of $CD27^{high}CD38^{high}CD180^{-}$ cells within $CD19^{+}$ cells from HS, seropositive patients, and CMS patients (**$P < 0.01$; Tukey's post hoc test). (*C*) Comparison of remission and relapse of NMO. Data obtained from the same patients are connected with lines (*$P < 0.05$; Wilcoxon signed rank test).

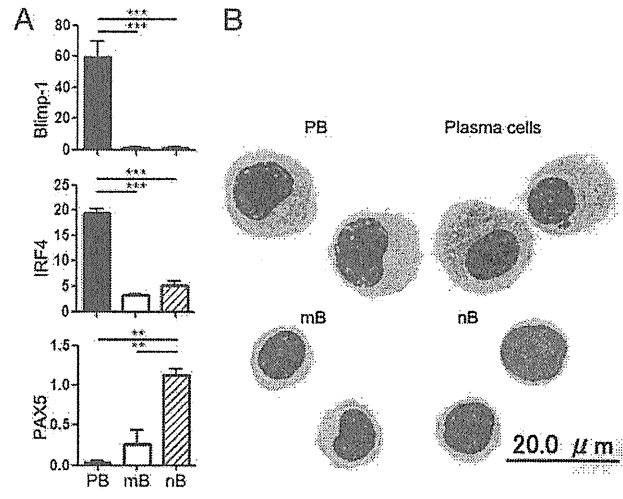

Fig. 2. Resemblance of $CD19^{int}CD27^{high}CD38^{high}CD180^{-}$ cells to plasma cells. (*A*) mRNA expression of Blimp-1, IRF4, and PAX5. B-cell subpopulations [$CD27^{high}CD38^{high}CD180^{-}$ (PB), $CD27^{-}$ naïve (nB), $CD27^{+}CD38^{-low}$ memory (mB)] were sorted by FACS and total RNA was extracted for qRT-PCR analysis. RNA levels were normalized to ACTB for each sample (**$P < 0.01$; ***$P < 0.001$; Tukey's post hoc test). (*B*) May–Grünwald–Giemsa staining of B-cell subpopulations. PB (*Upper Left*), mB (*Lower Left*), and nB (*Lower Right*) from NMO are presented along with morphologically identified plasma cells ($CD19^{int}CD27^{high}CD38^{high}CD138^{+}$) from HS (*Upper Right*).